Bioactive Materials 43 (2025) 98–113

Contents lists available at ScienceDirect

Bioactive Materials

journal homepage: www.keaipublishing.com/en/journals/bioactive-materials

Synthetic helical peptides on nanofibers to activate cell-surface receptors and synergistically enhance critical-sized bone defect regeneration

Tongqing Zhou [a], Rafael C. Cavalcante [b], Chunxi Ge [c], Renny T. Franceschi [c,e], Peter X. Ma [a,b,d,e,*]

[a] Macromolecular Science and Engineering Center, University of Michigan, Ann Arbor, MI 48109, USA
[b] Department of Biologic and Materials Sciences & Prosthodontics, University of Michigan, Ann Arbor, MI 48109, USA
[c] Department of Periodontics and Oral Medicine, University of Michigan, Ann Arbor, MI 48109, USA
[d] Department of Materials Science and Engineering, University of Michigan, Ann Arbor, MI 48109, USA
[e] Department of Biomedical Engineering, University of Michigan, Ann Arbor, MI 48109, USA

ARTICLE INFO

Keywords:
Nanofiber
Scaffold
Peptide
Discoidin domain receptor
Bone tissue engineering

ABSTRACT

More than 500,000 bone grafting procedures are performed annually in the USA. Considering the significant limitations of available bone grafts, we previously invented a phase-separation technology to generate nanofibrous poly(L-lactic acid) (PLLA) scaffolds that mimic the bone matrix collagen in nanofiber geometry and enhance bone regeneration. Here we report the development of nanofibrous scaffolds with covalently attached synthetic peptides that mimic native collagen peptides to activate the two main collagen receptors in bone cells, discoidin domain receptor 2 (DDR2) and β1 integrins. We synthesized a PLLA-based graft-copolymer to enable covalent peptide conjugation via a click reaction. Using PLLA and the graft-copolymer, we developed 3D scaffolds with interconnected pores and peptides-containing nanofibers to activate DDR2 and β1 integrins of osteogenic cells. The degradation rate and mechanical properties of the scaffolds are tunable. The peptides-decorated nanofibrous scaffolds demonstrated 7.8 times more mineralized bone regeneration over the control scaffolds without the peptides in a critical-sized bone defect regeneration model after 8 weeks of implantation, showing a synergistic effect of the two peptides. This study demonstrates the power of scaffolds to mimic ECM at both nanometer and molecular levels, activating cell surface receptors to liberate the innate regenerative potential of host stem/progenitor cells.

1. Introduction

Bone is a highly dynamic tissue with microscale fractures forming and healing continuously. However, a bone defect beyond a certain size scale is unable to self-heal and therefore a bone graft is required. There are about 2.2 million cases of bone grafting procedures carried out annually in the world, with more than 500,000 cases and a total expense of 5 billion dollars on bone grafting annually in the USA alone [1–3]. Among bone grafts, autografts are the gold standard, but the source of tissue is limited to the available bone of the patients themselves. Allografts and xenografts risk infection and host rejection. Tissue engineered bone grafts constructed using scaffolds with or without pre-seeded osteogenic cells have received increasing attention [4–7]. Their reduced immunogenicity is advantageous over allografts or xenografts while their off-the-shelf nature compensates for the limited availability of autografts. Basic requirements for a desired scaffold include biocompatibility, biodegradability, osteogenic activities, adequate mechanical properties to maintain the 3D shape for bone regeneration, porous structure enhancing vascularization and tissue regeneration, and the possibility to present biomolecules to promote osteogenesis [8–13].

Among various materials used in bone tissue engineering scaffolds, polyesters including polycaprolactone (PCL), poly(lactic acid) (PLA), poly(glycolic acid) (PGA) and poly(lactic-co-glycolic acid) (PLGA) are a group of FDA-approved polymeric materials that are promising candidates for potential clinical applications due to their biocompatibility and biodegradability. Various microstructures of bone regeneration

Peer review under responsibility of KeAi Communications Co., Ltd.
* Corresponding author. Department of Biologic and Materials Sciences & Prosthodontics 1011 North University Ave., Room 2211 The University of Michigan, Ann Arbor, MI 48109-1078, USA.
E-mail address: mapx@umich.edu (P.X. Ma).

https://doi.org/10.1016/j.bioactmat.2024.08.017
Received 30 June 2024; Received in revised form 15 August 2024; Accepted 17 August 2024

scaffolds have been achieved by different manufacturing techniques including porogen leaching [9,14–16], freeze drying [17], solid-liquid or liquid-liquid phase separation [18–21], electrospinning [22–24] or 3D printing [14,25,26]. Nano-scale fibers with similar geometry to that of collagen fibers, the major components of extracellular matrix (ECM) with a typical diameter of 50–500 nm, are found to be a desirable morphology and have been fabricated using electrospinning or thermally induced phase separation procedures (TIPS) [18,19,21,25]. Our laboratory developed a novel phase-separation technique to generate polymer scaffolds with several desired features including nanofibrous morphology and controllable 3D pore structures. The nanofibrous morphology of these PLLA scaffolds mimics collagen fibers in shape and dimensions. These scaffolds have been used for bone tissue engineering with demonstrated mechanical support and enhanced osteogenic properties [27–32].

In addition to its nanofibrous structure, a major factor contributing to the bioactivity of collagen is the presence within its triple helical structure of peptide sequences interacting with specific cell-surface receptors. The peptide sequence GFOGER (O = hydroxyproline), which binds β1 integrins, is known to increase cell adhesion and the expression of osteoblast-specific genes [33]. This peptide promoted osteogenic behavior when physically absorbed on a solid PCL scaffold or attached on a hydrogel [34,35]. We recently discovered that a second collagen receptor, discoidin domain receptor 2 (DDR2), also plays a vital role in bone development where it largely functions in skeletal progenitor cells (SPCs) to promote cell proliferation and osteogenic differentiation [36–40]. Human and mouse loss-of-function mutations in *DDR2* cause severe craniofacial and skeletal defects [36,41,42]. DDR2 binds the sequence, GVMGFO (O = hydroxyproline), which is present in fibrillar collagens. However, such peptides do not bind integrins or directly stimulate integrin activity, but rather increase integrin-mediated downstream signaling [43]. Significantly, seeding SPCs on tissue culture surfaces adsorbed with the DDR2-binding GVMGFO-containing triple-helical peptides stimulates osteoblast differentiation to a greater extent than surfaces adsorbed with β1 integrin-binding GFOGER peptides. Combined exposure of cells to both GVMGFO and GFOGER peptides stimulates more osteoblast differentiation and mineralization than individual peptides [44]. None of these bone cell receptor-binding peptides have been previously conjugated to a nanofiber. Our bone tissue engineering studies using 3D nanofibrous scaffold, studies of DDR2 in bone development, and preliminary cell culture data on peptides-absorbed plates lead us to hypothesize that synthetic biodegradable nanofibers decorated with a combination of DDR2-activating and integrin-activating triple-helical peptides may mimic key biological functions of collagen fibers in osteogenesis to synergistically enhance bone regeneration.

In the present study, we tested this hypothesis by first developing a novel approach to synthesize peptide-conjugated nanofibrous PLLA-based polymer scaffolds, to examine their activation of DDR2 and β1 integrin, and to evaluate their function in enhancing bone regeneration. A major challenge for this study was to design a PLLA-based polymer that allows controllable attachment of peptides while maintaining nanofiber-forming properties of PLLA. Pure PLLA lacks reactive functional groups and needs further functionalization for biomolecule attachments [45]. Here we reported a new 3D scaffold design from a blend of PLLA and PLLA-based graft copolymer, poly(2-hydroxyethyl methacrylate-graft-PLLA)-methacrylate (PHEMA-g-PLLA-ma), where the PLLA molecular weight, the PLLA chain length in the graft polymer, the feeding ratio of HEMA and graft polymer, and the blend ratio of PHEMA-g-PLLA-ma to PLLA were tailored to achieve the desired nanofibrous morphology, mechanical properties and peptide conjugation. The peptides-decorated nanofibrous scaffolds were evaluated for bone regeneration using a critical-sized bone defect regeneration model, and, excitingly, the individual and synergistic effects of GFOGER and GVMGFO peptides on bone regeneration were confirmed.

2. Results

2.1. Synthesis of poly(HEMA-graft-PLLA)-methacrylate (PHEMA-g-PLLA-ma)

PHEMA-g-PLLA-ma was synthesized with a route similar to our previous publication [46], illustrated in Scheme 1. HEMA-PLLA with different molecular weights was polymerized with L-lactide as the monomer and HEMA as the initiator. The resulting macromonomer was copolymerized with HEMA, followed by functionalization with methacrylate. The change of double bond was confirmed using both NMR (Fig. 1A–C) and FTIR (Fig. 1D–F). The peptide conjugation was also confirmed using FTIR (Fig. 1G).

2.2. The effect of PHEMA-g-PLLA-ma/PLLA blend ratio on physical and chemical properties of nanofibrous films

The newly synthesized PHEMA-g-PLLA-ma (Fig. 2A) was blended with pure PLLA to provide similar mechanical properties and morphology of pure PLLA nanofibers. A very high blend ratio of PHEMA-g-PLLA-ma/PLLA, such as above 50/50, resulted in either non-fibrous morphology or loss of typical nanofibrous morphology (became merged fibers) after phase separation (Fig. 2B), and thus was not further studied. All other characterizations were performed with lower blend ratios (≤50 %) (Table S1). A general trend among all the samples was that increasing the blend ratio from 10/90 to 50/50 decreased melting enthalpy and tensile modulus (Table S1, Fig. 2C), indicating lower crystallinity of the materials, likely due to the increasing amorphous HEMA content. In contrast, peptide conjugation density increased with increasing HEMA/L-lactide ratio since each HEMA segment brings one binding site, the methacrylate end group. The peptide conjugation density increased with increasing blend ratio.

When the grafted PLLA chain length in PHEMA-g-PLLA-ma was long enough, the tensile modulus no longer significantly decreased with increasing blend ratio, and similar tensile behavior to pure PLLA was shown even at 50/50 blend (Fig. 2D, Fig. S1). This suggested that the PLLA graft chain length played an important role in the mechanical properties of nanofibrous structure. It was likely that the long PLLA graft chain contributed to crystallinity and overall mechanical properties, where the polymer blend maintains similar physical properties as pure PLLA even at high PHEMA-g-PLLA-ma/PLLA blend ratio, corroborated by DSC data (Table S1).

2.3. The effect of PHEMA-g-PLLA-ma molecular design on physical and chemical properties of nanofibrous films

The effects of HEMA/L-lactide feed ratio on copolymerization and graft PLLA chain length were studied (Fig. 3A). At a fixed PHEMA-g-PLLA-ma/PLLA blend ratio where a typical nanofibrous morphology was maintained, the trends of modulus and peptide conjugation density were similar against the HEMA/L-lactide feed ratio, i.e., the modulus decreased with increasing HEMA/L-lactide ratios, and the conjugation density increased with increasing HEMA/L-lactide ratios (Table S1). At the highest PHEMA-g-PLLA-ma/PLLA blend ratio (50/50) maintaining a typical nanofibrous morphology, there were the greatest differences in modulus and conjugation density between the two HEMA/L-lactide feed ratios (0.43 vs 0.86) (Fig. 3B). Increasing HEMA/L-lactide feed ratio is always beneficial to conjugation density because more HEMA units contribute to more conjugation sites (methacrylate groups). Increasing graft PLLA chain length resulted in higher modulus, possibly due to improved crystallization of PLLA (higher crystallinity and larger crystal size) (Fig. 3C). The explanation was corroborated by the trend of increasing melting enthalpy when the graft PLLA chain was longer (Fig. S2). However, increasing graft PLLA chain length reduced peptide conjugation density (Fig. 3D). This change could be explained by the difference in the methacrylate groups available for conjugation reaction.

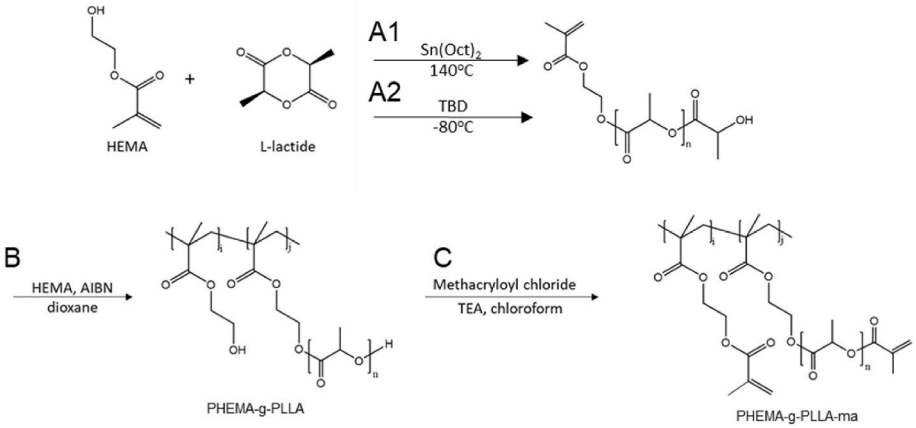

Scheme 1. Synthesis route of PHEMA-g-PLLA-ma. **A1)** and **A2)** Synthesis of macromolecule HEMA-PLLA of various molecular weights: **A1)** for lower molecular weight (<20k) and **A2)** for higher molecular weight (>20k). **B)** Copolymerization of HEMA-PLLA and HEMA. **C)** Functionalization of the terminal hydroxyl group by methacrylate.

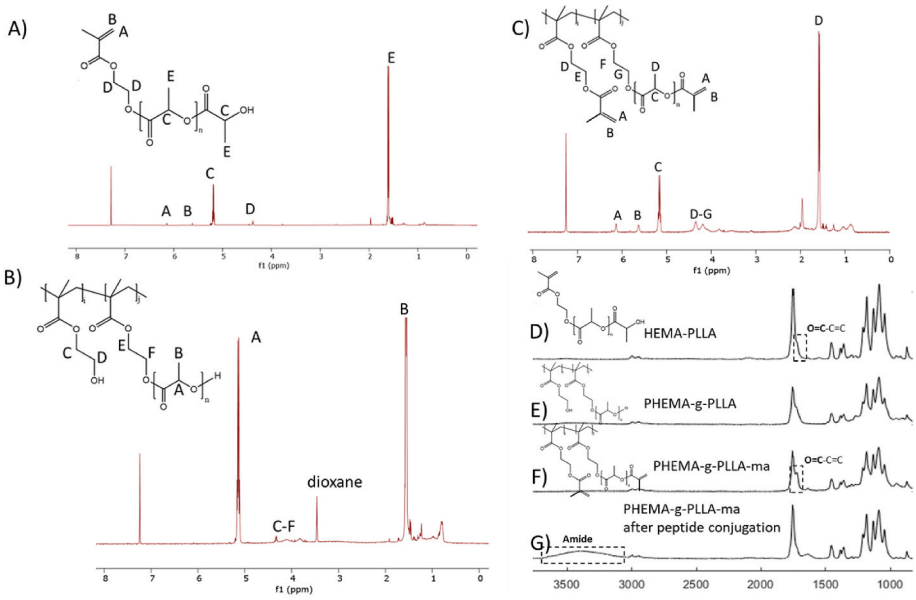

Fig. 1. Characterization of PHEMA-g-PLLA-ma and related compounds. **1A-C)** H NMR spectrum for HEMA-PLLA (**1A**), PHEMA-g-PLLA (**1B**) and PHEMA-g-PLLA-ma (**1C**). **1D-G)** ATR-FTIR spectrum for HEMA-PLLA (**1D**), PHEMA-g-PLLA (**1E**), PHEMA-g-PLLA-ma (**1F**) and PHEMA-g-PLLA-ma 3D scaffold after peptide conjugation and intensive wash (**1G**).

The methacrylate groups were presented at each HEMA unit and at the end of graft PLLA chain as well. The shorter the graft PLLA chain, the more methacrylate groups per mass of graft copolymer, resulting in a higher conjugation density. In addition, the comparison of molecular weight between PHEMA-g-PLLA-ma and graft PLLA chain confirmed that there were potentially more graft PLLA chains per graft copolymer when a shorter graft PLLA chain was used (Fig. S3). For a longer graft PLLA chain, the total number of methacrylate groups was smaller, therefore the conjugation density decreased with the increasing chain length (Fig. 3D).

2.4. Selection of PHEMA-g-PLLA-ma/PLLA blend composition

There are three variables that control the composition of PHEMA-g-PLLA-ma/PLLA blend: The blend ratio of PHEMA-g-PLLA-ma/PLLA, length of graft PLLA chain and ratio of HEMA/L-lactide in the graft copolymer. There are also three important features of the generated scaffolds, including the nanofiber features (morphology and diameter), mechanical properties such as modulus, and the achievable peptide conjugation density of the scaffolds. Based on our examination, polymer blend ratios lower than 50/50 ensure typical nanofiber morphologies which are known to enhance bone regeneration [47]. Therefore, we focus on scaffolds with polymer blend ratios ranging from 10/90 to 50/50. The two remaining criteria, modulus, and peptide conjugation density, are both important. Higher modulus can better maintain pore shape and size, which are known to affect vascularization and osteogenic differentiation [30]. The conjugation density determines how much peptide can interact with surface receptors and regulate cell behavior. The two criteria are displayed in the same graph and scaffolds with the highest conjugation densities at a given modulus are selected as candidates (red dots in Fig. 4).

The five selected blend compositions are all good scaffolds with comparable modulus to the pure PLLA scaffold and desired high peptide conjugation densities. Among these candidate scaffolds, the modulus and the conjugation density change in opposite directions. We selected a scaffold in the middle with balanced modulus and conjugation density

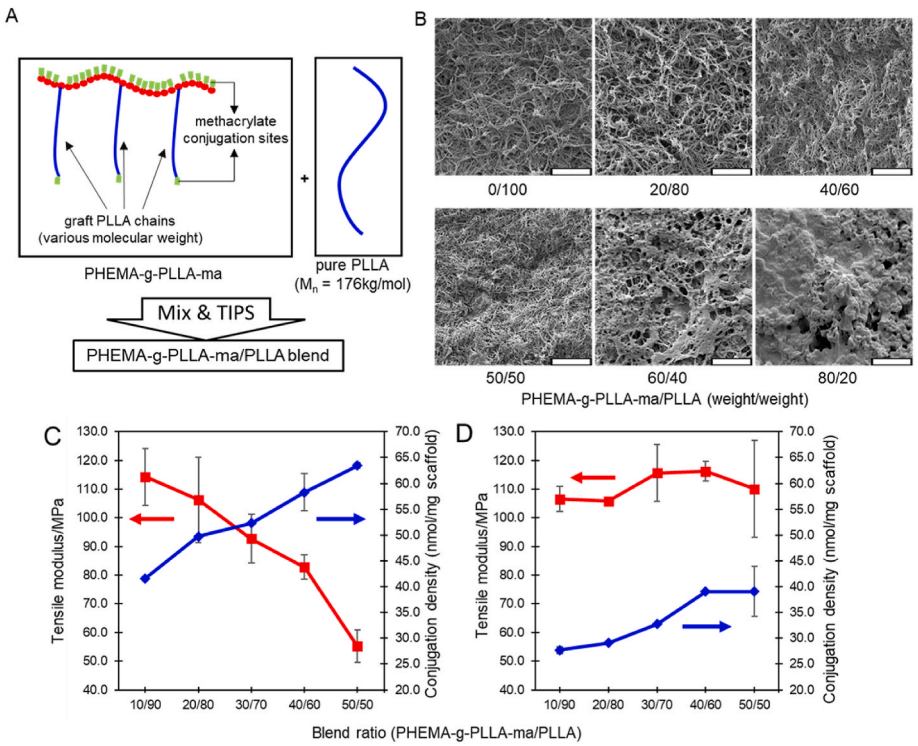

Fig. 2. Effect of blend ratio on tensile modulus (red) and peptide conjugation density (blue). **A)** Schematic illustration of polymer blend composition of PHEMA-g-PLLA-ma/PLLA blend, where: blue – PLLA chain, red – HEMA, green -methacrylate. **B)** Change of fibrous morphology with blend ratio (scale bar = 10 μm). **C)** The general trend of nanofibrous film tensile modulus and 3D scaffold peptide conjugation properties changes with increasing blend ratio. Polymer composition: 3.6k PLLA chain length, HEMA/L-lactide feed weight ratio 0.43. **D)** One special case: mechanical properties did not decrease when the blend ratio was increased. Polymer composition: 228k PLLA chain length, HEMA/L-lactide feed weight ratio 0.43. Stress-strain curves of **C)** and **D)** can be found in Fig. S1. (A colored version of this figure is available online).

for subsequent further in vitro and in vivo evaluations (PLLA chain length 3.6k, HEMA/L-lactide feed weight ratio 0.43, PHEMA-g-PLLA-ma/PLLA blend weight ratio 20/80).

To examine biocompatibility, 10k mouse BMSCs were seeded onto each PHEMA-g-PLLA-ma/PLLA blend scaffold with the selected polymer blend composition. Cell number (converted from total DNA content) increased with culture time, reaching about 4.6 times of the seeded cell number at 3 weeks (Fig. S4). This indicated that the PHEMA-g-PLLA-ma/PLLA blend 3D scaffold had good cell compatibility and supported cell proliferation, which is suitable for us to advance to subsequent peptide modification studies.

2.5. Qualitative and quantitative analyses of peptide conjugation

To conjugate peptides to scaffolds, we applied a well-established thiol-ene click reaction [48,49]. The covalent conjugation of peptides was identified by FTIR spectrum, where the C=C double bond decrease and amide region show up on 3D scaffold samples (Fig. 1G). To visualize peptide conjugation, two different peptides, GER and GVM, were conjugated on PHEMA-g-PLLA-ma films or 3D porous scaffolds with composition selected in **2.4** under UV light with a photo-initiator, IC2959. The conjugation ratio of peptides was controlled by varying the feeding ratio of peptides and visualized with their fluorescent light intensities from the 3D nanofibrous scaffolds (Fig. 5A). The amount of a peptide conjugated was controlled by the amount of the peptide fed, as higher feeding resulted in higher peptide conjugation (Fig. 5B). The ratio of conjugated peptide over fed peptide (conjugation percentage) was around 40 %–50 % when fed peptide was at the range of 0.9–9 nmol/mg (Fig. 5C). GER and GVM had similar conjugation reactivity (Fig. S5).

To further validate the persistence of covalent conjugation, GER-biotin-conjugated film was compared with physical absorption in terms of peptide retention in PBS solution over time (Fig. 5D, Fig. S6). The absorption was conducted by soaking nanofibrous films with the same peptide concentration as covalent conjugation at 4 °C overnight and was compared with covalently conjugated GER-biotin after 15-min incubation under UV with an initiator. The films were placed in a PBS solution at 37 °C for up to 3 weeks with PBS changed every day. The amount of remaining peptide was visualized by the intensity of fluorescence after staining with Streptavidin-Alexa Fluor 555 conjugate. After 1 day and 3 weeks, the remaining peptide in the physical adsorption group decreased substantially, while the fluorescence intensity from the covalently conjugated group did not change significantly. The result confirmed the covalent conjugation of peptides.

2.6. The degradation properties of 3D PHEMA-g-PLLA-ma/PLLA blend scaffolds

To evaluate the degradation of 3D scaffolds to be implanted, disk-shaped 3D porous nanofibrous scaffolds with a diameter of 18 mm and a thickness of 2 mm were fabricated with the selected polymer blend. The scaffolds were incubated in PBS at 37 °C for up to 8 weeks (10 ml PBS per scaffold, changed every day). SEM images indicated that the pore surfaces of both types of scaffolds became more porous at 2 weeks and lost mechanical integrity at 8 weeks. However, the PHEMA-g-PLLA-ma/PLLA blend scaffolds degraded faster than those of pure PLLA scaffolds (Fig. 6A). The mass loss of the PHEMA-g-PLLA-ma/PLLA blend scaffolds was substantially faster than that of pure PLLA scaffolds, which is desirable for our tissue engineering application. The mass loss data of the blend scaffolds at every time point (from 1 to 8 weeks) were statistically significantly lower than those of the control pure PLLA scaffolds ($p < 0.001$). The HEMA portion of the polymer was more

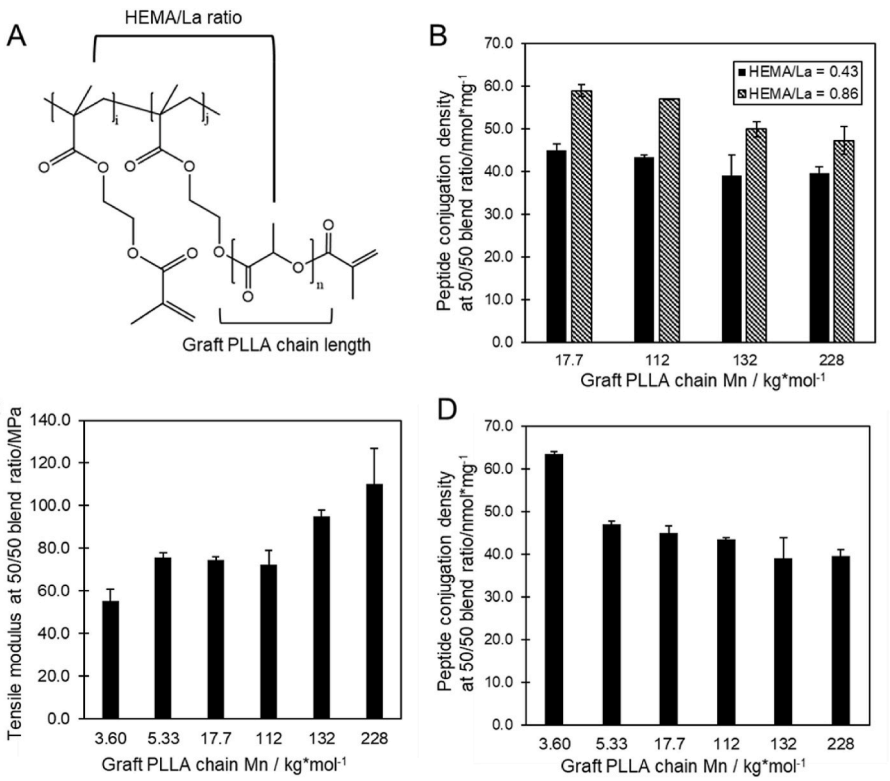

Fig. 3. Effect of PLLA chain length and HEMA/La weight ratio on tensile modulus (N = 3) and peptide conjugation density when PHEMA-g-PLLA-ma/PLLA blend ratio was 50/50 (N = 3). **A)** Illustration of HEMA/La ratio and PLLA chain length in PHEMA-g-PLLA-ma copolymer. **B)** The effect of HEMA/L-lactide weight ratio on peptide conjugation of 3D scaffolds, comparing different PLLA chain lengths. **C)** and **D)** Effect of PLLA chain length on modulus **(C)** and peptide conjugation density **(D)**, where HEMA/L-lactide weight ratios were fixed at 0.43.

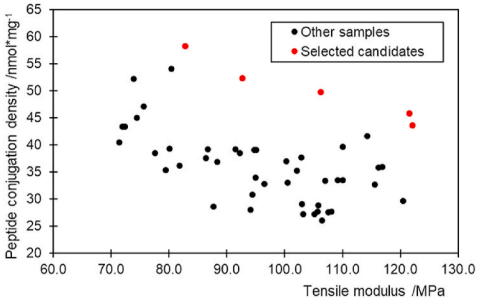

PHEMA-g-PLLA-ma group name*	PLLA chain Mn /g*mol^{-1}	HEMA/L-lactide weight ratio	blend ratio Polymer/PLLA	Tensile modulus /MPa	Conjugation /nmol*mg^{-1}
A	3.60k	0.43	40/60	82.8±4.2	58.3±3.6
A	3.60k	0.43	30/70	92.7±8.5	52.3±0.2
A	3.60k	0.43	20/80	106.2±14.9	49.8±0.1
E2	132k	0.86	50/50	121.6±14.2	45.8±1.6
D2	112k	0.86	10/90	122.1±13.4	43.6±9.2
Reference					
PLLA	-	-	0/100	110.3±3.6	-

Fig. 4. Tensile modulus and peptide conjugation density plot for PHEMA-g-PLLA-ma/PLLA blend scaffolds. A full list of fabricated scaffolds can be found in Table S1. (A colored version of this figure is available online).

hydrophilic and amorphous, contributing to a faster degradation rate compared to pure PLLA even when 80 % of the polymer blend was pure PLLA (Fig. 6B).

2.7. *In vitro differentiation of cell-seeded scaffolds*

The effect of peptide conjugation in vitro was demonstrated by seeding an immortalized cell line of human BMSCs at 500k/scaffold and cultured in an osteogenic medium. Four groups of PHEMA-g-PLLA-ma/PLLA blend 3D scaffolds with the selected peptide compositions were used: control, 100 μg GER per scaffold, 100 μg GVM per scaffold and 100 μg GER +100 μg GVM per scaffold. The peptide density calculation method was described in supplementary material **S2**. An increase in osteogenic gene expression was observed for peptide-conjugated scaffolds, including Runx2, ALP, BSP, OCN, Col1, and ColX (endochondral ossification). The GER + GVM scaffolds showed the most increase among all groups two weeks after seeding (Fig. S7). Also, a similar pattern of increase in vascularization gene expression was shown. Peptide-conjugated scaffolds improved Pecam1 (Cd31) and Cd34 expression two weeks after seeding, and the GER + GVM group displayed higher expression than the other groups (Fig. S8).

Among the osteogenic markers we observed, the increase of Runx2, BSP, OCN, and Col1 expressions was consistent with other in vitro studies, which validated the bioactivity of GER peptide [50–52]. Since GVM, the DDR2-binding peptide, was never conjugated on a 3D scaffold, we would also like to confirm that GVM peptide activated DDR2 of the cells. Immunofluorescence staining using human phospho-DDR1/DDR2 antibody (pDDR, R&D Systems) was conducted, and we observed that cell-seeded scaffolds with GVM peptide conjugation displayed signals around the nuclei of cells after two weeks of culture, suggesting the activation of DDR (Fig. 7).

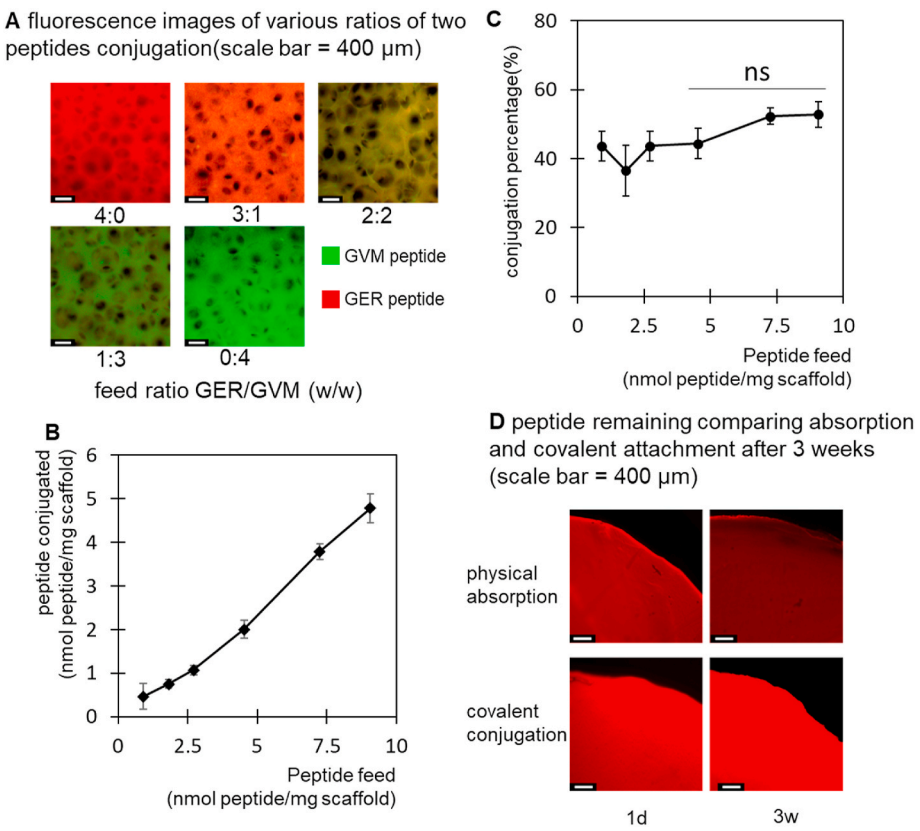

Fig. 5. Qualitative and quantitative evaluations of peptide conjugation on PHEMA-g-PLLA-ma/PLLA blend films or 3D porous scaffolds with selected polymer blend composition from **2.4**. **A)** The control of GER/GVM peptide ratio by controlling feed ratio. **B)** Peptide conjugation vs. peptide feeding, and **C)** Peptide conjugation percentage of feed peptide amount measured by quantification kit (GER peptides were used for quantification). **D)** Fluorescence visualization of peptide surface density changes from 1 day to 3 weeks in PBS (1 ml PBS per film, changed every day), comparing physical absorption with covalent conjugation. Quantitative comparison was done using a method described in supplementary data S1 and results were shown in Fig. S6. (A colored version of this figure is available online).

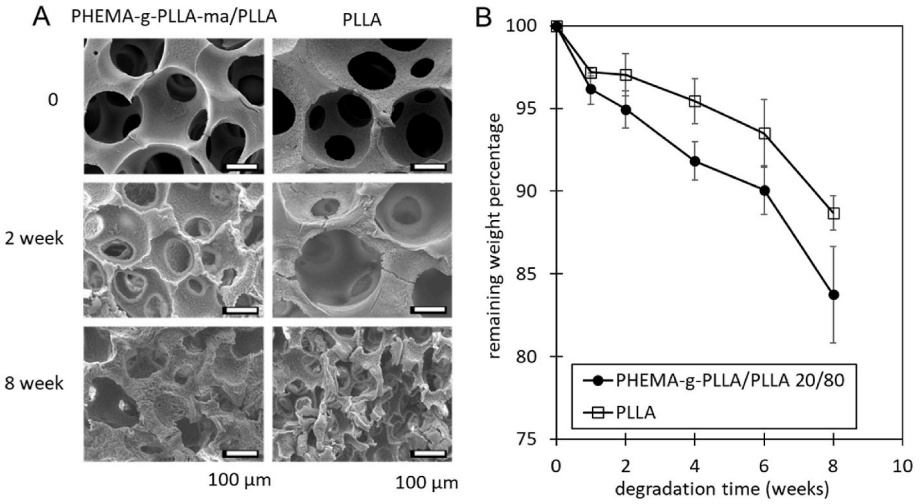

Fig. 6. Degradation properties of 3D porous PHEMA-g-PLLA-ma/PLLA blend scaffolds. Each scaffold was soaked in 10 ml PBS at 37 °C, where PBS was changed every day. **A)** SEM images during the 8-week degradation (scale bar: 100 μm). **B)** Weight changes during 8-week degradation. The selected polymer blend composition in 2.4 was used.

2.8. Evaluation of peptide-conjugated nanofibrous scaffolds using a mouse critical-sized calvarial bone defect regeneration model

Four groups of PHEMA-g-PLLA-ma/PLLA blend 3D scaffolds with the selected peptide compositions were used: control, 100 μg GER per scaffold, 100 μg GVM per scaffold and 100 μg GER +100 μg GVM per scaffold. Scaffolds were implanted in critical-sized calvarial defects, and skulls were harvested after 4 weeks and 8 weeks. Regenerated bone volume was measured in the defects using Micro-CT analysis (Fig. 8A). Each peptide group showed significantly more bone volume from their own 4-week to 8-week time points, suggesting continuous bone regeneration over time (Fig. 8B). At 8 weeks, there were significant

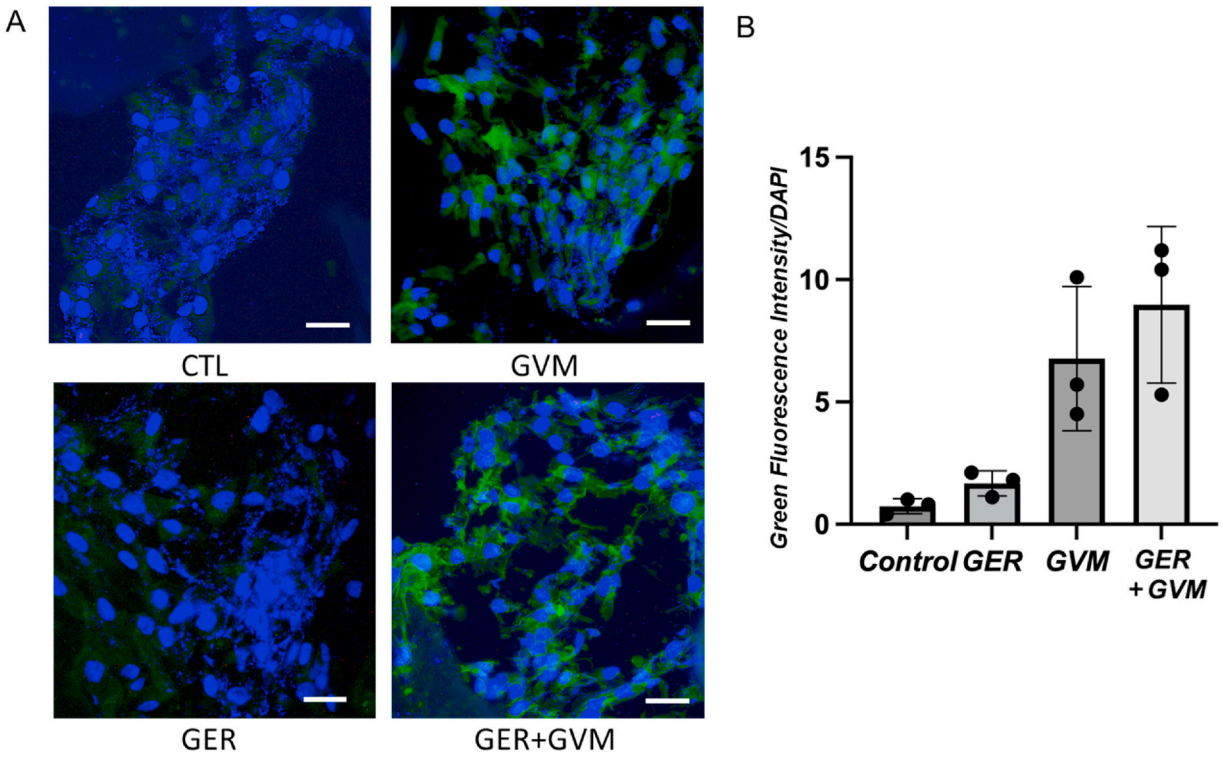

Fig. 7. Activation of DDR on human BMSCs seeded on 3D porous scaffolds with IF staining of pDDR as primary antibody after two weeks. (A) IF images of pDDR (stained green, AlexaFluor 488) and cell nuclei (stained blue, DAPI), scale bar = 50 μm. (B) Quantification of green fluorescence intensity over blue intensity (DAPI). $p = 0.0073$ (**) according to one-way ANOVA. Polymer blend composition: 3.6k PLLA chain length, HEMA/PLLA feed weight ratio 0.43, PHEMA-g-PLLA-ma/PLLA blend weight ratio 20/80.
CTR: Control 3D scaffolds without peptide conjugation (click reaction condition applied as other groups).
GER: Scaffolds with 100 μg GER peptide as feed for conjugation per scaffold.
GVM: Scaffolds with 100 μg GVM peptide as feed for conjugation per scaffold.
GER + GVM: Scaffolds with 100 μg GER and 100 μg GVM peptide as feed for conjugation per scaffold.

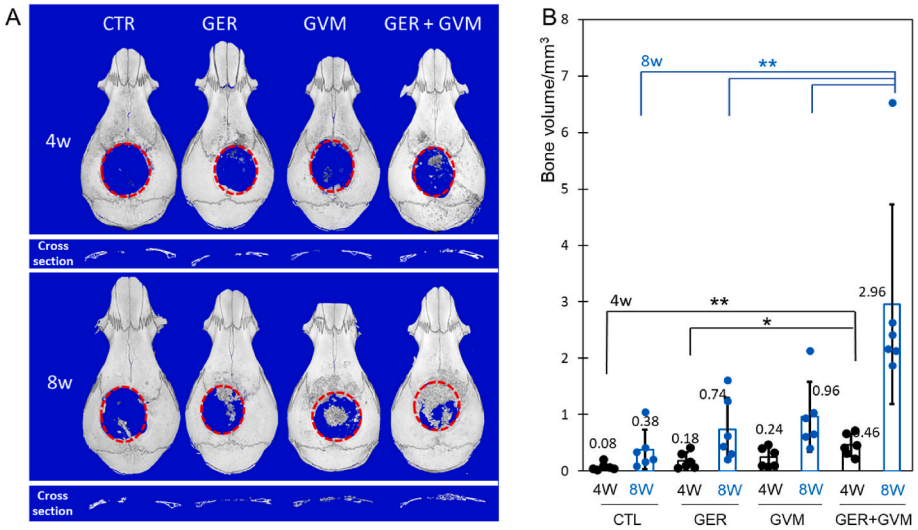

Fig. 8. Micro-CT images and bone volume analysis on 4-week and 8-week mouse critical-sized calvarial bone defect repair with cell-free 3D scaffold implantation. **A)** Micro-CT images with top view and cross-section view. **B)** Bone volume/mm^3, One-way ANOVA was used to access significance from multiple comparisons. *$p \leq 0.05$, **$p \leq 0.01$. The selected polymer blend composition from Section 3.5 was used. Scaffold dimensions: 5 mm in diameter, 1 mm in thickness, with pore size of 250–425 μm. Six animals were used for each group. (A colored version of this figure is available online).
CTR: Control 3D scaffolds without peptide conjugation (click reaction condition applied as other groups).
GER: Scaffolds with 100 μg GER peptide for conjugation per scaffold.
GVM: Scaffolds with 100 μg GVM peptide for conjugation per scaffold.
GER + GVM: Scaffolds with 100 μg GER and 100 μg GVM peptides for conjugation per scaffold.

differences ($p < 0.05$) in bone volume between the GER + GVM group and other groups, control, GER, and GVM (Fig. 8B). At 4 weeks, there were significant differences ($p < 0.05$) in bone volume between the GER + GVM group and two other groups, GER and control (Fig. 8B). The bone volumes of GER + GVM groups were not only the highest among all groups, but also higher than the combined bone volumes obtained with the two individual peptides. At 4 weeks, the bone volume of the both-peptide group was 6.0 times of the control group, which was equal to 2.6 times of GER alone, 1.9 times of GVM alone, and 1.1 times of the sum of GER and GVM. At 8 weeks, the bone volume of the both-peptide group was 7.8 times that of the control group, which was equal to 4.0 times the GER alone group, 3.1 times the GVM alone group, and 1.7 times the sum of GER and GVM alone groups. Six animals were used for each group.

Histologic images showed a similar trend as micro-CT image. Four weeks after implantation, Hematoxylin and Eosin (H&E) and Masson's Trichrome (MT) staining showed more bone formation in the group with both peptides, while bone formation in three other groups was minimal (Fig. 9A), where arrows indicate new bone domains and blue color indicates new collagen deposition measured by trichrome staining. There were also cartilage-like regions (marked with C in trichrome staining) in the single peptide groups at 4 weeks. Eight weeks after implantation, large areas of more mature bone formed, particularly in the groups with both peptides (arrows), while less bone formation was observed for the single peptide groups (arrows). The lowest bone and the lowest new collagen matrix deposition was seen in the control group (Fig. 9B). These findings were consistent with micro-CT results and suggested that GER and GVM peptides on nanofibers of the 3D scaffolds synergistically enhanced bone regeneration.

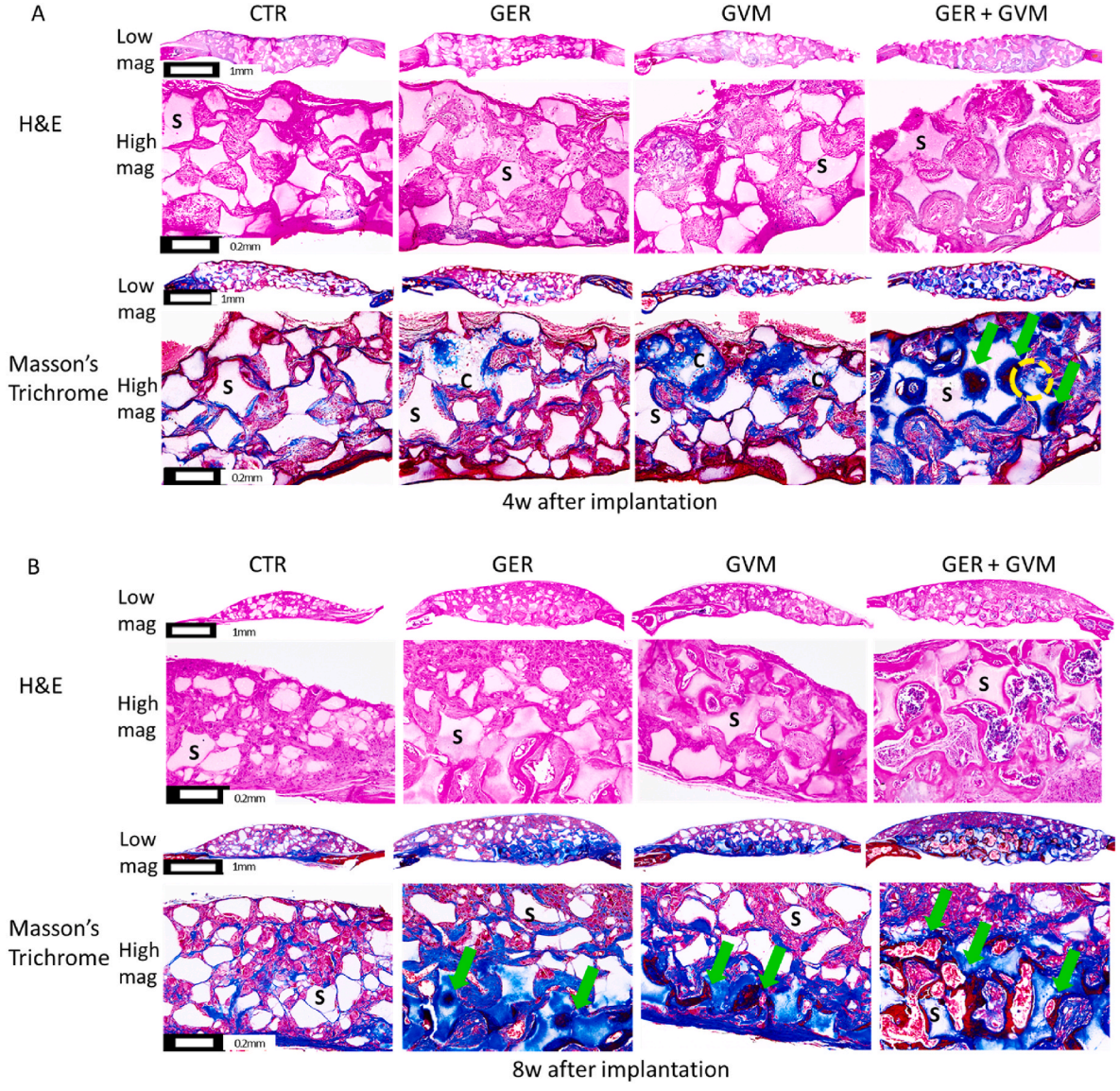

Fig. 9. H&E staining and Masson's trichrome staining on paraffin-embedded sections of implanted 3D scaffolds in mouse critical-sized calvarial bone defects. A) 4 weeks after implantation and B) 8 weeks after implantation. Green arrows pointed to new bone areas, blue showed new collagen deposition, the letter 'S' indicated scaffold areas, and the letter 'C' indicated cartilage-like structures (A colored version of this figure is available online).
CTR: Control 3D scaffolds without peptide conjugation (click reaction condition applied as other groups).
GER: Scaffolds with 100 μg GER peptide as feed for conjugation per scaffold.
GVM: Scaffolds with 100 μg GVM peptide as feed for conjugation per scaffold.
GER + GVM: Scaffolds with 100 μg GER and 100 μg GVM peptide as feed for conjugation per scaffold.

2.9. Immunofluorescence (IF) imaging of peptide effects on tissue regeneration

Following H&E and MT staining, we assessed the efficacy of peptide-conjugated scaffolds in facilitating the ingrowth of blood capillaries and in supporting the formation of bone and cartilage tissue. Four weeks post-implantation, immunofluorescence analysis with antibodies to endothelial markers, CD31 (Fig. 10) and Von Willebrand Factor (VWF, Fig. S9), showed clusters of endothelial cells, indicative of vascularization, with a consistent distribution pattern. Notably, there was unremoved host tissue on the outer surface of scaffold implants, such as in the control group in Fig. 9 (CTL-4w). We focused on examining the new vessel formation inside the scaffold implants. Scaffolds incorporating both peptide types were associated with an elevation in both CD31 and VWF immunofluorescence in comparison to the control group or to those scaffolds conjugated with a single type of peptide, suggesting enhanced angiogenic response. After eight weeks, this trend was amplified. The scaffolds containing a combination of peptides exhibited a substantial enrichment of fluorescence within the marrow-like structures located at the central areas of the scaffolds. The distribution of both CD31 and VWF was predominantly observed encircling the newly formed blood vessels as pointed out by the arrows, indicating neovascularization (Fig. 10, Fig. S9). This suggests that the dual-peptide scaffolds may modulate a favorable microenvironment that promotes angiogenesis more effectively than the scaffolds containing a single peptide.

The increased accumulation of CD31 and VWF around the marrow-like structures and along the new vessels implies a successful integration of the scaffold with the host's vasculature, which is crucial for nutrient and oxygen supply to the regenerating tissue. Furthermore, the enhanced angiogenic activity alongside the marrow-like structures could indicate a stimulatory interaction between the scaffold and the host's regenerative processes, potentially leading to more efficient osteogenesis. The synergistic effect of the combined peptides might be directing the scaffold to support a more organized tissue architecture mimicking the native bone.

IF staining for SRY-box transcription factor 9 (*Sox9*) revealed that this chondrogenic marker was localized primarily around the marrow-like structures within the scaffolds (Fig. 11). Four weeks post-implantation, chondrocyte-like structures were found with concentrated Sox9 signals (Arrows in Fig. 11). The scaffolds that were conjugated with both types of peptides demonstrated an enhanced fluorescent signal in comparison to the controls or those conjugated with a single type of peptide. This suggests a more robust chondrogenic phenotype in the peptide-conjugated scaffolds, especially dual-peptide-conjugated scaffolds. By the eighth week, there were remaining fluorescent signals of *Sox9*, which were predominantly observed within the central marrow-like structures of the scaffolds (Fig. 11).

Staining for Runt-related transcription factor 2 (*Runx2*), a marker associated with osteogenic differentiation, was analyzed (Fig. 12). At the four-week time point, Runx2 was more prominently observed in the group of scaffolds that were conjugated with both peptides, indicating enhanced osteogenic activity. Additionally, scaffolds conjugated solely with the peptide GVM displayed a notable increase in the level of fluorescence, suggesting a positive osteogenic response attributable to DDR2 activation.

This trend continued at 8 weeks where overall Runx2 staining increased in all groups, but particularly in the GER plus GVM peptide group.

3. Discussion

While more than 500,000 of bone grafting procedures are performed annually in the USA, there are substantial limitations and concerns over

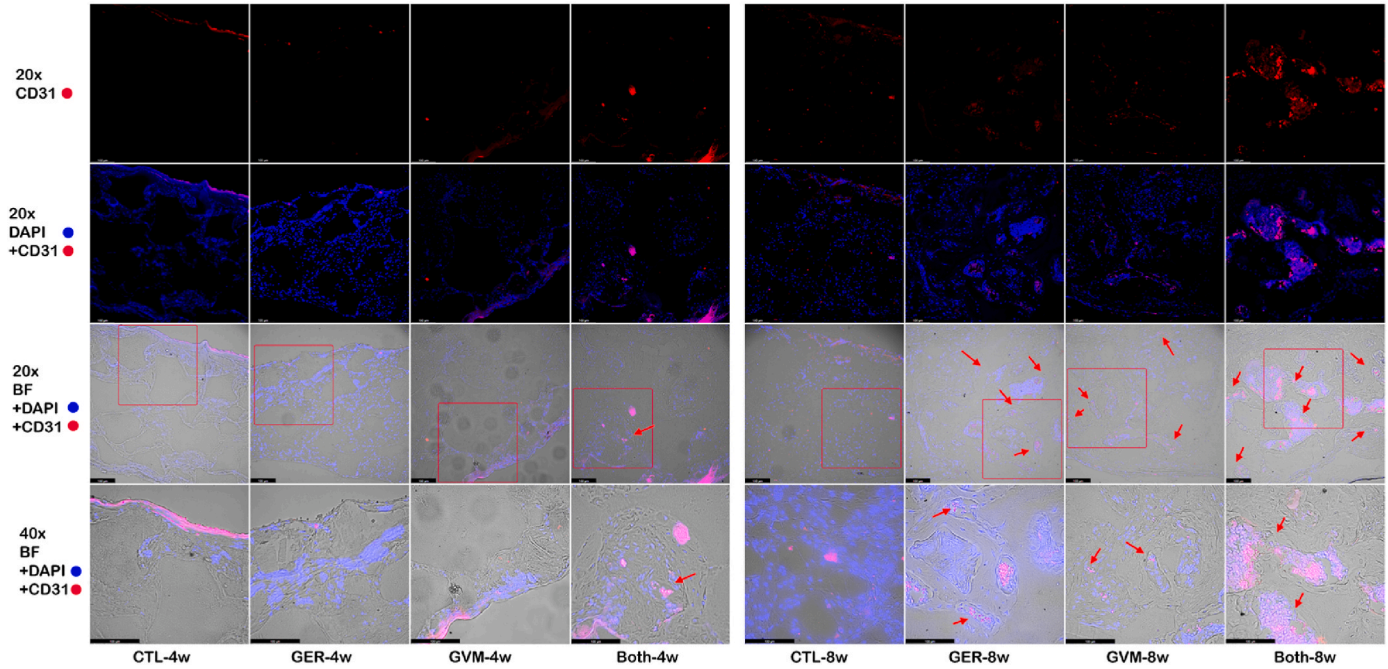

Fig. 10. Neovascularization was examined using IF staining of CD31 positive endothelial cells in cell-free 3D scaffolds harvested 4 or 8 weeks after implantation in mouse critical-sized calvaria defects. CD31 was stained red (AlexaFluor 594), and cell nuclei were stained blue (DAPI). Bright field images were superimposed on IF staining in row 3. Row 4 is higher mag images of row 3 (red boxes). Scale bar = 100μm. (A colored version of this figure is available online).
Groups for this and all following IF staining images:
CTR: Control 3D scaffolds without peptide conjugation.
GER: Scaffolds with 100 μg GER peptide as feed for conjugation per scaffold.
GVM: Scaffolds with 100 μg GVM peptide as feed for conjugation per scaffold.
Both: Scaffolds with 100 μg GER and 100 μg GVM peptide as feed for conjugation per scaffold.

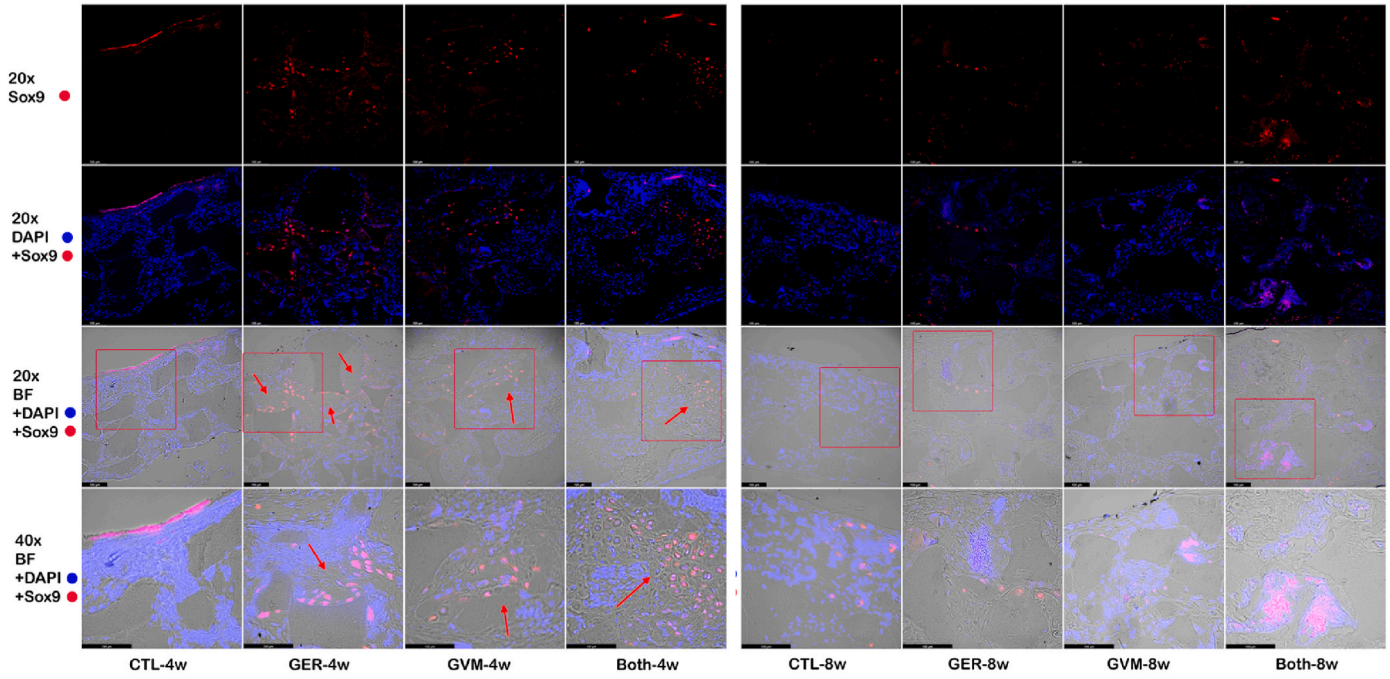

Fig. 11. IF staining for *Sox9* of cell-free 3D scaffolds harvested 4 or 8 weeks after implantation in mouse critical-sized calvarial defects. *Sox9* was stained red (AlexaFluor 594), and cell nuclei were stained blue (DAPI). Bright-field images were superimposed on IF staining in row 3. Row 4 is higher mag images of row 3 (red boxes). Arrows indicate chondrocyte-like regions with *Sox9* signal. Scale bar = 100μm. (A colored version of this figure is available online).

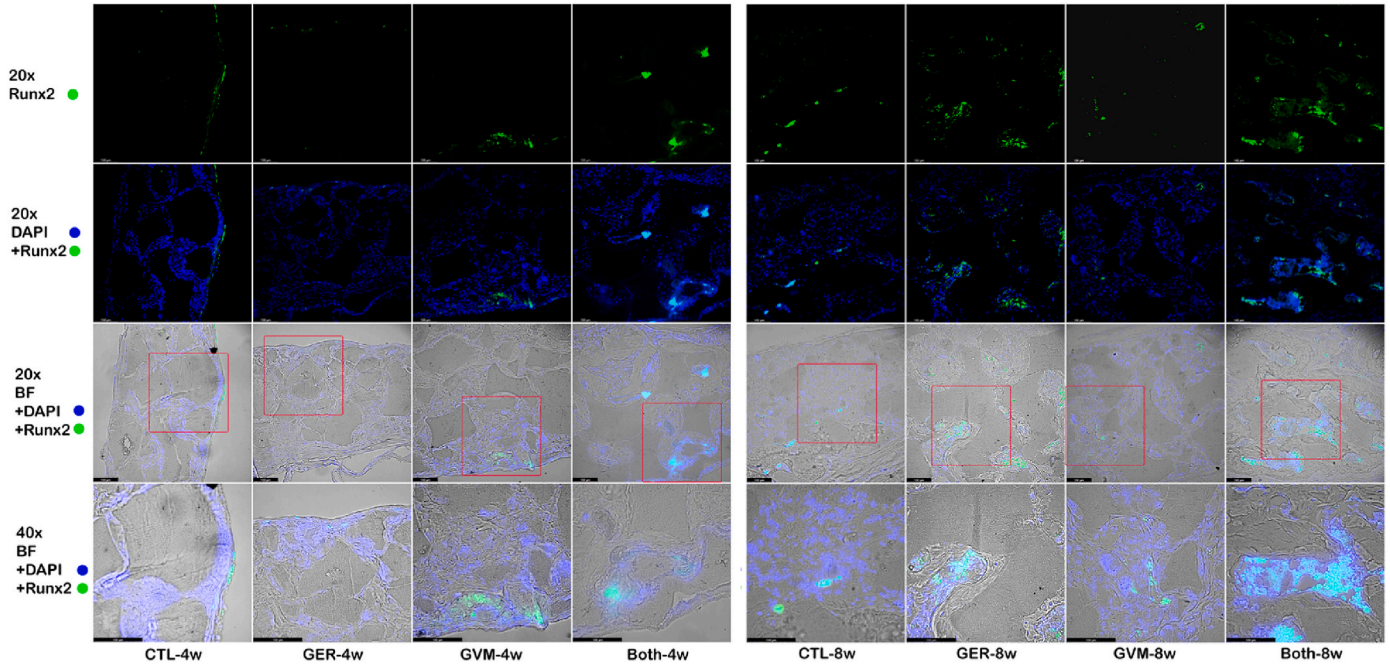

Fig. 12. IF staining for *Runx2* in cell-free 3D scaffolds harvested at 4 or 8 weeks after implantation in mouse critical-sized calvarial defects. *Runx2* was stained green (AlexaFluor 488), and cell nuclei were stained blue (DAPI). Bright field images were superimposed on IF staining in row 3. Row 4 is higher mag images of row 3 (red boxes). Scale bar = 100μm. (A colored version of this figure is available online).

the currently available bone grafts [1–3]. PLLA is an FDA-approved material with various medical uses including as screws and plates for bone fixation and is biocompatible and biodegradable. Our lab developed a novel phase-separation technology to fabricate nanofibrous PLLA scaffolds that mimic the collagen of the organic bone matrix in fiber diameter and geometry [19]. Furthermore, we developed several ways to generate controlled pore sizes and shapes into such nanofibrous scaffolds as well control overall anatomic geometries at the macroscopic levels [25,53,54]. These nanofibrous scaffolds were shown to enhance bone regeneration through improved protein adsorption and cell-matrix interactions [47,55]. However, these scaffolds differ from native collagen in that they do not contain biomolecules on the nanofibers that can directly interact with collagen receptors on osteogenic cells.

In this study, we developed nanofibrous scaffolds containing synthetic triple-helical peptides that mimic native collagen by activating the two major cell surface collagen receptors in bone cells, β1 integrins

and the DDR2. To achieve this, it was first necessary to add functional groups on the PLLA polymer chains without compromising their capacity to form nanofibers. We, therefore, synthesized a graft-copolymer, PHEMA-g-PLLA-ma in this study (Fig. 1), to utilize the functionality of methacrylate in the repeating HEMA units and the end groups of the graft PLLA chains for peptide conjugation by the thiol-ene click reaction.

However, in addition to introducing functional groups for peptide conjugation, the copolymerization also introduced grafted polymer chains and could result in shorter graft PLLA chain lengths, which can compromise the capacity for polymer chain crystallization and nanofiber formation. We systematically synthesized many such graft copolymers by varying HEMA and LLA contents and chain lengths, where we obtained a library of graft copolymers to achieve varying functionalities and structures (Fig. S1). We also visualized the covalently conjugated peptides and their ratios in 3D nanofibrous scaffolds as well as demonstrated their long-term presence on the scaffolds (Fig. 5).

We also wanted to maintain the good mechanical properties and to achieve desired degradation kinetics of the new scaffolds. Instead of using the graft copolymer PHEMA-g-PLLA-ma alone, we prepared polymer blends of PHEMA-g-PLLA-ma and pure PLLA (Fig. S1). It is confirmed that tunable peptide ratios can be achieved along with the desired nanofibrous morphology of the scaffolds when the graft copolymer content is 50 % or lower (Fig. 2). When the blend ratio is fixed, it was found that higher HEMA content improves peptide conjugation capacity, and higher PLLA content in the graft copolymer improves mechanical properties (Figs. 3 and 4). The longer graft PLLA chain length contributes to better mechanical properties and shorter graft PLLA chains contribute to higher peptide conjugation properties. While many of the synthesized graft copolymer compositions and blend ratios resulted in satisfactory nanofiber formation, good mechanical properties, and conjugation capacity, we focused on one of the new nanofibrous scaffolds with balanced higher conjugation capacity and satisfactory mechanical properties for further evaluations.

As we know, bone tissue engineering scaffolds should maintain their porous 3D structure for cell population and construction of premature tissue and degrade at the stage when mature tissue forms [56]. According to previous studies from our lab, 8 weeks is the usual time when mature bone tissue starts to form in critical-sized calvaria defect models [29,57,58]. Therefore, we examined the degradation behaviors of the new scaffolds over 8 weeks. Satisfactory degradation behavior was achieved where the porous structure of scaffolds remained intact over a few weeks (Fig. 6). The hydrophilicity of the HEMA component in the graft copolymer likely led to faster degradation rates.

To determine if the conjugated peptides on the nanofibrous scaffolds can enhance osteogenic differentiation of BMSCs, we conducted in vitro differentiation studies and quantified gene expressions. We showed that 3D scaffolds with peptide conjugation enhanced the expression of osteogenic markers and vascularization markers, where the scaffolds with both peptides showed the highest expressions (Figs. S7–S8). DDR2-binding peptide was never conjugated on 3D scaffolds before. To provide direct proof of DDR activation, we performed immunofluorescence staining using pDDR antibody, and the results showed significantly higher pDDR signals in scaffolds with DDR2-binding peptide (Fig. 7). This data provided us with confidence to advance the project to in situ bone regeneration studies.

Using a critical-sized mouse calvarial defect regeneration model where the defect cannot spontaneously heal, we evaluated the performance of the newly developed helical peptide-decorated cell surface receptor-activating nanofibrous scaffolds for bone regeneration. Excitingly, it was demonstrated that the new nanofibrous scaffolds with either of the two peptides (DDR2 or β1 integrin activating) significantly improved bone regeneration outcome based on both histological analyses and micro-CT analysis compared to the control nanofibrous scaffolds. DDR2 activating peptide had a more significant effect than the β1 integrin activating peptide in enhancing bone regeneration on the nanofibrous scaffolds. More excitingly, the dual peptide decorated nanofibrous scaffolds regenerated a mineralized bone volume that was 7.8 times that of the control nanofibrous scaffolds after 8 weeks of implantation, which is 1.7 times of the summation of two single peptide-conjugated scaffolds (Fig. 8), indicating a synergistic effect of the DDR2 and β1 integrin activating peptides. While it will be important to investigate the molecular mechanisms of the synergy between the two receptor-activating peptides in enhancing mineralized bone regeneration in future studies, the present data firmly supports our hypothesis that nanofibers decorated with either of the two triple-helical peptides may mimic key biological functions of collagen fibers to enhance bone regeneration, and nanofibers decorated with both peptides synergistically enhance osteogenic properties and therefore substantially further facilitate bone regeneration. The H&E and Trichrome staining was consistent with the micro-CT analysis, showing cellular and matrix distribution in the regenerated 3D tissue constructs (Fig. 9).

Since it is well known that bone regeneration requires vascularization, the neovascularization has been examined using immunofluorescence staining, showing a consistent trend between mineralization and neovascularization in these scaffolds in response to the conjugated collagen-mimicking synthetic peptides (Fig. 10 and Fig. S9).

Literature tells us that calvarial bone is formed via intramembranous mineralization during development. However, in the present study it was observed that there were more chondrocyte-like cells and cartilage-like matrix in earlier stages of implantation (4 weeks) or less stimulating environments (such as scaffolds conjugated with single peptide, compared to those conjugated both peptides). However, the chondrocyte-like cells and cartilage-like matrix appeared to decrease at 8 weeks when vascularized and mineralized bone formation increased (Figs. 9–12). This observation supports a process more consistent with endochondral bone formation during scaffold-supported bone regeneration. This observation was corroborated by previous studies showing that a low level of transient chondrogenic gene expression occurs during normal calvarial development and that this increases under altered biological conditions such as craniosynostosis [40,59].

Interestingly, we also observed a continued presence of chondrocyte-like cells and cartilage-like matrix in the marrow-like structures of the regenerated calvarial bone from these peptide-conjugated scaffolds. This result suggests that the mesenchymal stem/progenitor cells in the marrow of the regenerated calvarial bone retain their multi-lineage differentiation potentials, showing both chondrocyte-like and osteoblast-like differentiation potentials even at later times, similar to those in the marrow of long bones [60].

Nanofibrous 3D scaffolds with similar fiber size to that of natural collagen promote osteogenic properties [61]. Integrin-binding and DDR2-binding peptides are sequences derived from natural collagen promoting osteogenic differentiation [2]. In our new scaffold, the polymeric part provided structure support and non-specific surface interaction while the peptides provided specific binding to cell receptors. We demonstrated that a combination of peptides and nanofibrous 3D scaffolds greatly enhanced the osteogenic gene expression in vitro and promoted bone tissue regeneration in vivo. Although cell interaction mechanisms with peptides on nanofibrous scaffolds could be complex, the nanofibrous 3D scaffolds with controllable peptide conjugation techniques will help to further understand such mechanisms in the future.

4. Conclusion

In this study, we synthesized a series of PLLA-based graft copolymers PHEMA-g-PLLA-ma, and successfully fabricated 3D porous PHEMA-g-PLLA-ma/PLLA blend nanofibrous scaffolds. The methacrylate group in the graft copolymer enabled thiol-ene click reaction to achieve covalent peptide conjugation on nanofibers of the scaffolds. The PLLA portion of the blend and the graft PLLA chains in the copolymers contributed to the formation of the nanofibrous structure and retaining satisfactory mechanical properties. The effect of molecular composition

of the graft copolymer was investigated and optimized for nanofiber morphology, mechanical properties, and peptide conjugation capacity. Controllable and persistent peptide presentation was achieved. Discoidin domain receptor 2 (DDR2) binding peptide and integrin binding peptide were used to functionalize nanofibrous PLLA scaffolds for the first time. The osteogenic effect of the newly designed DDR2 activating and integrin activating 3D nanofibrous scaffolds was evaluated using a mouse critical-sized bone defect regeneration model. The effect of the dual peptides conjugated nanofibrous scaffold on bone volume regeneration was 7.8 times that of the control scaffold and 1.7 times that of the summation of the single peptide-conjugated nanofibrous scaffolds after 8 weeks of implantation, indicating a synergistic effect in vivo. As a versatile 3D nanofibrous scaffold design with click-reaction capacity, PHEMA-g-PLLA-ma/PLLA blend scaffolds have exciting potential for regeneration of bone and other tissues. This study convincingly demonstrates the importance and power of scaffolds to mimic ECM at both nanometer and molecular levels, e.g. to activate two cell surface receptors in this novel approach to liberate the innate regenerative power of host stem/progenitor cells.

5. Experimental section

5.1. Materials

Poly(L-lactide) (referred to as pure PLLA, Resomer® L 207 S, Mn = 176k), L-lactide (La), azobisisobutyronitrile (AIBN), 1,4-dioxane, methanol, dichloromethane (DCM), triethylamine (TEA), methacryloyl chloride, tetrahydrofuran (THF), ethanol, mineral oil, sodium hydrogen carbonate ($NaHCO_3$), anhydrous sodium sulfate, Tin(II) 2-ethylhexanoate ($Sn(Oct)_2$), hydroxyethyl-methacrylate (HEMA), triazabicyclodecene (TBD), Span 80®, anhydrous sodium sulfate, Irgacure 2959 were purchased from Sigma-Aldrich Company (USA). D-fructose was purchased from Oakwood Chemical. Hydrochloric acid (HCl), fructose, phosphate buffered saline (PBS), sodium chloride (NaCl), saline, ethylenediaminetetraacetic acid (EDTA) and tromethamine (Tris) were purchased from Thermo Fisher Scientific (USA). Custom peptides were purchased from Alan Scientific (US) (Table 1). C57BL/6J mice (female) of 6-to-8-week-old were purchased from The Jackson Laboratory. The β1 integrin-activating peptide GFOGER (GER), DDR2-activating GVMGFO (GVM), and GFOGER-biotin (GER-biotin) peptide were purchased from Alan Scientific (US) (95 % purity with trifluoroacetate removal service). Hydrogen peroxide (30 %) was purchased from Supelco. Diva Decloaker (10X) was purchased from BIOCARE MEDICAL. All primary antibodies and secondary antibodies were purchased from Cell Signaling Technology. Normal donkey serum (NDS) was purchased from the Colorado Serum Company. Triton was purchased from Promega Corp. Formalin (10 %) was purchased from Sigma. ProLong™ Gold antifade reagent with DAPI (DAPI mounting solution) was purchased from Fisher.

5.2. Synthesis of hydroxyethyl-methacrylate-poly(L-lactide) (HEMA-PLLA) macromonomer (molecular weight <20,000 g/mol)

Fixed mole ratio of L-lactide and HEMA were added into a 100 ml round-bottomed flask. $Sn(Oct)_2$ with 0.01 mol% of L-lactide is added as the catalyst. The flask was sealed, and nitrogen gas was used to purge the container for 10 min. The container was put onto a glycerol bath at 140 °C for 2 h during which the reaction mixture turned from a transparent liquid to a white, opaque, viscous liquid. The container was then cooled down to room temperature. Dichloromethane was added to dissolve the mixture. Precipitate was removed by centrifugation. Polymer/dichloromethane solution was added into cold methanol (1:10 vol ratio) and immediately centrifuged. The white precipitate was washed with methanol 2 more times and Milli-Q Water 3 times, and then freeze-dried to form white solid product, hydroxyethyl-methacrylate-poly(L-lactide) (HEMA-PLLA).

5.3. Synthesis of hydroxyethyl-methacrylate-poly(L-lactide) (HEMA-PLLA) macromonomer (molecular weight >20,000 g/mol)

TBD, L-lactide, and HEMA were pre-dried with anhydrous sodium sulfate prior to the reaction. A 20 ml vial with 1.5 g of molecular sieve was sealed and underwent nitrogen gas purge for 10 min 10 wt% of L-lactide pre-dissolved in anhydrous DCM with HEMA of 1/100 to 1/800 mol ratio to L-lactide was added in the vial using a syringe. A syringe loaded with 2 mg/ml TBD solution (0.1mol% of L-lactide) was set on the rubber cover with a Teflon filter. The device was cooled down at −80 °C for 1 h before TBD solution was injected into the vial. The vial was set at −80 °C for 48 h. The viscous reaction mixture was put on rotary evaporator to remove DCM. The product was washed off from molecular sieve using an excess amount of DCM and vacuum dried to remove DCM. The monomer was washed away with ethyl acetate 2 times before the product was dried to form transparent-to-opaque white film, hydroxyethyl-methacrylate-poly(L-lactide) (HEMA-PLLA).

5.4. Synthesis of poly(hydroxyethyl-methacrylate)-graft-PLLA (PHEMA-g-PLLA)

HEMA-PLLA macromonomer was dissolved in 1,4-dioxane with a weight percentage of 10 % under 60 °C until it is completely dissolved. The solution was added into a 100 ml round-bottomed flask with various amounts of HEMA and AIBN in 1,4-dioxane and was purged with nitrogen gas for 10 min. The weight ratio of HEMA, AIBN and macromonomer was typically 0.43/0.01/1 (mole ratio 50:1:5 when HEMA-PLLA molecular weight was 3000 g/mol). The flask was put onto a glycerol batch at 80 °C for 24 h. The transparent reaction mixture was then poured into cold methanol (1:10 vol ratio) and centrifuged. The white flocculent precipitate was then washed with methanol 2 more times and Milli-Q water 3 times, and then freeze-dried to form white solid product, poly(hydroxyethyl-methacrylate)-graft-PLLA (PHEMA-g-PLLA).

5.5. Synthesis of poly(HEMA-graft-PLLA)-methacrylate (PHEMA-g-PLLA-ma)

PHEMA-g-PLLA was dissolved in DCM (5 wt%) in a 100 ml round-bottomed flask. The flask was sealed and purged with nitrogen gas for 5 min, then placed in an ice-water bath for at least 10 min before the reaction. Triethylamine (TEA) was added into the flask first, and methacryloyl chloride was added into the flask drop-wise. Mole ratio of HEMA, AIBN and macromonomer was 2:1:1. The flask was kept in the ice-water bath for 1 h. The resulting liquid mixture with a slight red

Table 1
Sequences and names for peptides used.

Peptide sequence	Abbreviation	Source
GGPGPPGPPGPPGPPGPPGFOGERGPPGPPGPPGPPGPPGPPGPC-NH2 O=Hydroxyproline	GER	Alan Scientific Inc (US)
GPCGPPGPPGPPGPPGPPGPRGQOGV(Nle)GFOGPPGPPGPPGPPGPPGPPGGP-NH2	GVM	
GGPGPPGPPGPPGPPGPPGFOGERGPPGPPGPPGPPGPPGPPGPC-NH2-biotin O=Hydroxyproline	GER-biotin	

color was then washed with 50 ml 0.1M HCl 2 times until pH of the water phase dropped below 7, then washed with 50 ml 0.5M $NaHCO_3$ once. The organic phase was then poured into cold methanol (1:10 vol ratio) and centrifuged. The precipitate is washed with methanol 2 more times and Milli-Q water 3 times, and then freeze-dried to form white solid product, poly(HEMA-graft-PLLA)-methacrylate (PHEMA-g-PLLA-ma).

5.6. Nanofibrous film fabrication with PHEMA-g-PLLA-ma/PLLA blend

Nanofibrous films were prepared using a thermally induced phase separation method. 10 wt% of polymers with various weight ratios of PHEMA-g-PLLA-ma and PLLA were dissolved in tetrahydrofuran (THF) at 60 °C until the solution became transparent. The viscous polymer solution was then poured into a preheated 0.5-mm-thick mold made of two pieces of glass slides with silicon wafer as inner surface of the lower slide to ensure film flatness. The mold was immediately sealed afterward and placed into a −80 °C freezer for 2 days to induce phase separation. The mold was then unsealed and submerged in an ice-water batch to exchange THF. The solidified film was then dried between paper towels on benchtop and stored in vacuum until further experiments.

5.7. Nanofibrous 3D porous scaffold fabrication with PHEMA-g-PLLA-ma/PLLA blend

3D scaffolds were fabricated following a previous publication from our group [62]. Briefly, fructose microspheres used for 3D pore generation were formed by cooling down a fructose/mineral oil emulsion from 120 °C to ice-water bath and collecting fructose spheres with diameter of 250–425 μm using stainless steel sieves. The fructose spheres were submerged in hexane and annealed in a Teflon vial at 37 °C. The vial was then vacuum dried to remove hexane. 10 wt% of PHEMA-g-PLLA-ma/PLLA blends with various compositions were dissolved in THF at 60 °C. The viscous solution was injected into the Teflon vial with dry fructose template. A brief vacuum was used to remove air in the fructose template and allow polymer solution to fill the pores throughout. The vial was then sealed and placed in −80 °C freezer for 2 days. The vial was then unsealed, soaked into hexane to remove THF, and then soaked into water to remove fructose template. The porous 3D nanofibrous scaffold was collected, cut into desired shapes and freeze dried until further experiments.

5.8. Peptide conjugation on nanofibrous films or 3D porous scaffolds

A piece of 5-mm-diameter film (for visualization) or 5-mm-diameter 3D porous scaffold (for implant or peptide conjugation density measurements) was weighted to calculate peptide conjugation amount per mass. The piece was wet with ethanol in a cell culture plate for 30 min before reaction. 1:1 volume of two solutions, 1 wt% Irgacure 2959/methanol and 0.1∼1 mg/ml peptide/PBS, were added to the wetted film or 3D scaffolds, for a volume of 0.2 mL per piece. The plate was moved under a UV lamp and exposed to UV light for 15 min. Supernatant before and after reaction was collected for peptide consumption measurements and the film or 3D scaffold was washed with ethanol 3 times and PBS 3 times for 30 min each and stored at −80 °C until further experiments.

5.9. Polymer, film and scaffold characterizations

H^1 Nuclear Magnetic Resonance (H NMR): HEMA-PLLA, PHEMA-g-PLLA, PHEMA-g-PLLA-ma were dissolved in d-chloroform for a concentration of 5 w/v% and tested on Varian Inova 500 (500 MHz).

Fourier-Transform Infrared Spectroscopy (FTIR): HEMA-PLLA powder, PHEMA-g-PLLA powder and PHEMA-g-PLLA-ma/PLLA nanofibrous films before and after peptide conjugation was analyzed with Thermo-Nicolet IS-50 instrument with ATR-FTIR diamond crystal accessory.

Gel Permeation Chromatography (GPC): 0.5 mg/ml THF solution of polymer samples were filtered and analyzed on Shimadzu GPC to determine molecular weight using polystyrene standards.

Scanning Electron Microscopy (SEM): Film and scaffold samples underwent gold coating and were observed under JEOL JSM-7800FLV SEM instrument. The images were analyzed, and average fiber diameter was calculated by measuring 50–100 fibers for each sample.

Differential Scanning Calorimetry (DSC): A PerkinElmer DSC-7 Differential Scanning Calorimeter was used to obtain DSC data. 5∼10 mg of nanofibrous polymer films were added in an aluminum sample holder and were heated from 50 °C to 190 °C at a speed of 20 °C per minute. Melting enthalpy was calculated using the built-in area calculation of the program.

Film mechanical properties: Film samples were cut into sheets with 2 mm width and 20 mm length. The dimensions of individual specimens were measured by a caliper. A GT-UA03 Single Column Tensile Test Machine with a 50 N loading cell was used for all mechanical tests. The samples were fixed on a small force film holder with a 10 mm gauge length and extended at a speed of 0.5 mm/min. Tensile modulus and strain at break was calculated from stress-strain curve.

5.10. Peptide conjugation density determination

The amount of conjugated peptide (μg peptide per mg scaffold) was determined by subtracting remaining peptide and wash-away peptide from total feeding peptide. The conjugation percentage was given by the ratio of conjugated peptides to total feeding peptides. 0.1 ml peptide solution (1 mg/ml) was used for reaction. Concentrations were determined following the protocol provided by Pierce™ Quantitative Peptide Assays (Thermo Fisher Scientific) and were converted into molar amount of peptide per mass of a scaffold. The detailed calculation of peptide conjugation was described in supplementary data **S2.**

5.11. Visualization of peptide conjugation

Two different labeling techniques were used. GER-biotin peptide synthesized by the peptide provider was labeled by Streptavidin-Alexa Fluor 555 conjugate (Avidin-Alex, excitation/emission wavelength: 555/565 nm) after conjugation reaction with nanofibrous film or 3D scaffold. The other method was to label the amino terminal of peptide using Fluorescein isothiocyanate isomer I (FITC, excitation/emission wavelength: 495/519 nm) in pH 9.0 Phosphate buffer for 12 h, followed by dialysis purification. The FITC-labeled peptide was then conjugated to films or 3D scaffolds. A Leica Thunder microscope was used to observe the two dyes at corresponding wavelengths.

5.12. Degradation studies

3D porous scaffolds were cut into disks with a diameter of 18 mm and a thickness of 2 mm and were soaked in PBS (10 ml per disk, changed every day) at 37 °C for up to 8 weeks. 2–3 disks were used for each replicate and 3 replicates per timepoint were used for weight loss calculation. SEM images were taken at 3 timepoints: 0 week (before incubation), 2 weeks and 8 weeks of incubation, to examine surface morphology changes.

5.13. Cell proliferation

Mouse bone marrow-derived mesenchymal stem cells (BMSCs) were harvested from the legs of 6-to-8-week-old C57BL/6J female mice (four mice total, cells were combined after harvesting) and seeded on PHEMA-g-PLLA-ma/PLLA blend 3D scaffolds (5 mm diameter, 2 mm thickness), wetted with ethanol 3 times, PBS 3 times and α-MEM one time at a density of 10k cells per scaffold. Cell-seeded scaffolds were incubated with cell culture medium (α-MEM with 10 % FBS) at 37 °C for up to 3 weeks. Samples were collected at 4 h, 1 week, 2 weeks and 3 weeks after seeding. 150uL Tris-NaCl-EDTA (TNE) buffer and 10uL proteinase K (20

mg/ml) were used to remove protein at 55 °C for 24 h and was later precipitated by adding 6M NaCl solution. Supernatants were measured following the protocol of Quant-iT™ dsDNA Assay Kits. The cell number of each sample was determined by comparing the DNA concentration to cell standards with the number of cells acquired by hemocytometer [63].

5.14. In vivo bone regeneration with cell-free 3D scaffolds in a mouse critical-sized calvarial bone defect

The animal procedures were performed according to a protocol approved by the Institutional Animal Care & Use Committee (IACUC) of the University of Michigan (following the NIH Guidelines). C57BL/6J mice of 6-to-8-week-old were pre-injected with 5 mg/kg carprofen and anesthetized with isoflurane. The skull area was shaved and cleaned with iodine and saline solution. A 5-mm incision was made at the center line of the skull and a 5 mm-diameter trephine bur was used to carefully remove a round piece of bone. A cell-free PHEMA-g-PLLA-ma/PLLA blend scaffold with or without peptide conjugation wetted with saline was placed into the defect and silk suture was used to close the incision. Mice were sacrificed at 4-week and 8-week time points. Skulls were collected and underwent fixation in 4 % paraformaldehyde at 4 °C for 24 h. The samples were stored in 70 % ethanol before characterization. Six animals were used for each group.

5.15. Bone volume analysis

A micro-CT system (μCT100 Scanco Medical, Bassersdorf, Switzerland) was used to scan the samples under voxel size 18 μm, 70 kVp, 114 μA, 0.5 mm AL filter, and integration time of 500 ms. Results were processed using dragonfly software to calculate the bone volume in the defects (with a lower threshold of 18 % and an upper threshold of 100 %) [36,47].

5.16. Histology analysis

Samples after the micro-CT scan were cleaned by removing soft tissues around the scaffold and demineralized in 14 wt% EDTA solution (pH = 7.4) for 10 days. The samples were then embedded in paraffin, sliced (with a thickness of 10 μm), and stained following the standard protocol of H&E staining and Masson's trichrome staining.

5.17. Immunofluorescence (IF) imaging

Paraffin-embedded slides (with a thickness of 10 μm) were deparaffined and post-fixed in 10 % formalin for 10 min. The slides were then incubated in 3 % hydrogen peroxide for 5 min, washed with PBS 3 times (5 min each time), followed by antigen retrieval in Diva Decloaker solution (Biocare Medical) at 60 °C overnight. The slides were then cooled to room temperature, washed with PBS for 4 times with 5 min each time, and incubated with a PBS solution containing 0.1 % Triton, 0.1 % BSA, and 2 % NDS for 1 h. Primary rabbit antibodies bound to CD31, VWF, Sox9, or Runx2 markers (1:100 in 0.1 % Triton/PBS) were dropped on the slides and kept at 4 °C overnight before being rinsed with PBS for 4 times with 5 min each time. Afterward, Donkey-anti-rabbit secondary antibodies (Alexa Flour 594 or 488, 1:1000 in 0.1 % Triton/PBS) were dropped on the slides. The slides were incubated at room temperature for 2 h. PBS was used to wash away excess amounts of antibodies for 4 times with 5 min each time, and a DAPI mounting solution was dropped on the slides before a cover glass was placed on top of the slides. Images were taken using a Leica Thunder microscope. Overlapping of bright field image, DAPI fluorescence signal, and secondary antibody fluorescence signal were done using the build-in program in the microscope.

5.18. Statistical analysis

Sample data of polymer mechanical properties and fiber diameter, peptide conjugation and bone volume were presented as Mean ± standard deviation (SD). The student t-test was used to determine significance (two-tail, unpaired) between two groups. Ordinary one-way ANOVA was used to determine significance for multiple comparisons.

Data availability

The data that support the findings of this study are available from the corresponding author upon reasonable request.

Ethics approval and consent to participate

The animal procedures were performed according to a protocol approved by the Institutional Animal Care & Use Committee (IACUC) of the University of Michigan (following the NIH Guidelines).

CRediT authorship contribution statement

Tongqing Zhou: Writing – review & editing, Writing – original draft, Visualization, Methodology, Investigation, Formal analysis, Data curation, Conceptualization. **Rafael C. Cavalcante:** Writing – original draft, Methodology, Formal analysis, Data curation. **Chunxi Ge:** Methodology, Formal analysis. **Renny T. Franceschi:** Writing – review & editing, Resources, Methodology, Investigation, Funding acquisition, Formal analysis. **Peter X. Ma:** Writing – review & editing, Writing – original draft, Supervision, Resources, Project administration, Methodology, Investigation, Funding acquisition, Formal analysis, Conceptualization.

Declaration of competing interest

The authors declare the following financial interests/personal relationships which may be considered as potential competing interests: The authors believe there is no known conflict of interest related to this work. However, they want to indicate that the materials developed in this manuscript have been used to file an US patent and PCT applications by the University of Michigan.

Acknowledgements

The authors would like to acknowledge the financial support from Department of Defense (DoD W81XWH-20-1-0572: PXM; W81XWH-20-1-0571: RTF) and National Institutes of Health (NIH R01DE029465: RTF and R01AR075770: PXM). The authors would also like to thank Yu-Shan Chen, Alba Gutierrez Cucurull, and Marek Lee for their assistance.

Received: ((will be filled in by the editorial staff))

Revised: ((will be filled in by the editorial staff))

Published online: ((will be filled in by the editorial staff))

Appendix A. Supplementary data

Supplementary data to this article can be found online at https://doi.org/10.1016/j.bioactmat.2024.08.017.

References

[1] M. Braddock, P. Houston, C. Campbell, P. Ashcroft, Born again bone: tissue engineering for bone repair, Physiology 16 (5) (2001) 208–213, https://doi.org/10.1152/physiologyonline.2001.16.5.208.

[2] P.V. Giannoudis, H. Dinopoulos, E. Tsiridis, Bone substitutes: an update, Injury 36 (3) (2005) S20–S27, https://doi.org/10.1016/j.injury.2005.07.029.

[3] J.R. Perez, D. Kouroupis, D.J. Li, T.M. Best, L. Kaplan, D. Correa, Tissue engineering and cell-based therapies for fractures and bone defects, Front. Bioeng. Biotechnol. 6 (2018), https://doi.org/10.3389/fbioe.2018.00105.

[4] X. Liu, P.X. Ma, Polymeric scaffolds for bone tissue engineering, Ann. Biomed. Eng. 32 (3) (2004) 477–486, https://doi.org/10.1023/b:abme.0000017544.36001.8e.

[5] V. Campana, G. Milano, E. Pagano, M. Barba, C. Cicione, G. Salonna, W. Lattanzi, G. Logroscino, Bone substitutes in orthopaedic surgery: from basic science to clinical practice, J. Mater. Sci. Mater. Med. 25 (10) (2014) 2445–2461, https://doi.org/10.1007/s10856-014-5240-2.

[6] G. Fernandez de Grado, L. Keller, Y. Idoux-Gillet, Q. Wagner, A.-M. Musset, N. Benkirane-Jessel, F. Bornert, D. Offner, Bone substitutes: a review of their characteristics, clinical use, and perspectives for large bone defects management, J. Tissue Eng. 9 (2018) 204173141877681, https://doi.org/10.1177/2041731418776819.

[7] S. Fukuba, M. Okada, K. Nohara, T. Iwata, Alloplastic bone substitutes for periodontal and bone regeneration in dentistry: current status and prospects, Materials 14 (5) (2021) 1096, https://doi.org/10.3390/ma14051096.

[8] P.X. Ma, Scaffolds for tissue fabrication, Mater. Today 7 (5) (2004) 30–40, https://doi.org/10.1016/S1369-7021(04)00233-0.

[9] P.X. Ma, Tissue engineering, in: J.I. Kroschwitz (Ed.), Encyclopedia of Polymer Science and Technology, John Wiley & Sons, Inc., Hoboken, NJ, 2005, pp. 261–291.

[10] P.X. Ma, Biomimetic materials for tissue engineering, Adv. Drug Deliv. Rev. 60 (2) (2008) 184–198, https://doi.org/10.1016/j.addr.2007.08.041.

[11] J. Hu, P.X. Ma, Nano-fibrous tissue engineering scaffolds capable of growth factor delivery, Pharmaceut. Res. 28 (6) (2011) 1273–1281, https://doi.org/10.1007/s11095-011-0367-z.

[12] J.M. Holzwarth, P.X. Ma, Biomimetic nanofibrous scaffolds for bone tissue engineering, Biomaterials 32 (36) (2011) 9622–9629, https://doi.org/10.1016/j.biomaterials.2011.09.009.

[13] E.J. Lee, F.K. Kasper, A.G. Mikos, Biomaterials for tissue engineering, Ann. Biomed. Eng. 42 (2) (2014) 323–337, https://doi.org/10.1007/s10439-013-0859-6.

[14] A.G. Mikos, A.J. Thorsen, L.A. Czerwonka, Y. Bao, R. Langer, D.N. Winslow, J. P. Vacanti, Preparation and characterization of poly(l-lactic acid) foams, Polymer 35 (5) (1994) 1068–1077, https://doi.org/10.1016/0032-3861(94)90953-9.

[15] P.X. Ma, R. Langer, Fabrication of biodegradable polymer foams for cell transplantation and tissue engineering, in: J.R. Morgan, M.L. Yarmush (Eds.), Tissue Engineering Methods and Protocols, Humana Press, Totowa, NJ, 1999, pp. 47–56, https://doi.org/10.1385/0-89603-516-6:47.

[16] L. Lu, S.J. Peter, M.D. Lyman, H.-L. Lai, S.M. Leite, J.A. Tamada, J.P. Vacanti, R. Langer, A.G. Mikos, In vitro degradation of porous poly(l-lactic acid) foams, Biomaterials 21 (15) (2000) 1595–1605, https://doi.org/10.1016/S0142-9612(00)00048-X.

[17] M.-H. Ho, P.-Y. Kuo, H.-J. Hsieh, T.-Y. Hsien, L.-T. Hou, J.-Y. Lai, D.-M. Wang, Preparation of porous scaffolds by using freeze-extraction and freeze-gelation methods, Biomaterials 25 (1) (2004) 129–138, https://doi.org/10.1016/S0142-9612(03)00483-6.

[18] R. Zhang, P.X. Ma, Poly(α-hydroxyl acids)/hydroxyapatite porous composites for bone-tissue engineering. I. Preparation and morphology, J. Biomed. Mater. Res. 44 (4) (1999) 446–455, https://doi.org/10.1002/(SICI)1097-4636(19990315)44:4<446::AID-JBM11>3.0.CO;2-F.

[19] P.X. Ma, R. Zhang, Synthetic nano-scale fibrous extracellular matrix, J. Biomed. Mater. Res. 46(1) (1999) 60-72.https://doi.org/10.1002/(sici)1097-4636(199907)46:1<60:Aid-jbm7>3.0.Co;2-h.

[20] Y.S. Nam, T.G. Park, Porous biodegradable polymeric scaffolds prepared by thermally induced phase separation, J. Biomed. Mater. Res. 47 (1) (1999) 8–17, https://doi.org/10.1002/(sici)1097-4636(199910)47:1<8::aid-jbm2>3.0.co;2-l.

[21] P.X. Ma, R. Zhang, Microtubular architecture of biodegradable polymer scaffolds, J. Biomed. Mater. Res. 56 (4) (2001) 469–477, https://doi.org/10.1002/1097-4636(20010915)56:4<469::AID-JBM1118>3.0.CO;2-H.

[22] Z.-M. Huang, Y.Z. Zhang, M. Kotaki, S. Ramakrishna, A review on polymer nanofibers by electrospinning and their applications in nanocomposites, Compos. Sci. Technol. 63 (15) (2003) 2223–2253, https://doi.org/10.1016/S0266-3538(03)00178-7.

[23] C.Y. Xu, R. Inai, M. Kotaki, S. Ramakrishna, Aligned biodegradable nanofibrous structure: a potential scaffold for blood vessel engineering, Biomaterials 25 (5) (2004) 877–886, https://doi.org/10.1016/S0142-9612(03)00593-3.

[24] C.P. Barnes, S.A. Sell, E.D. Boland, D.G. Simpson, G.L. Bowlin, Nanofiber technology: designing the next generation of tissue engineering scaffolds, Adv. Drug Deliv. Rev. 59 (14) (2007) 1413–1433, https://doi.org/10.1016/j.addr.2007.04.022.

[25] V.J. Chen, L.A. Smith, P.X. Ma, Bone regeneration on computer-designed nano-fibrous scaffolds, Biomaterials 27 (21) (2006) 3973–3979, https://doi.org/10.1016/j.biomaterials.2006.02.043.

[26] F.J. Martínez-Vázquez, M.V. Cabañas, J.L. Paris, D. Lozano, M. Vallet-Regí, Fabrication of novel Si-doped hydroxyapatite/gelatine scaffolds by rapid prototyping for drug delivery and bone regeneration, Acta Biomater. 15 (2015) 200–209, https://doi.org/10.1016/j.actbio.2014.12.021.

[27] G. Wei, Q. Jin, W.V. Giannobile, P.X. Ma, The enhancement of osteogenesis by nano-fibrous scaffolds incorporating rhBMP-7 nanospheres, Biomaterials 28 (12) (2007) 2087–2096, https://doi.org/10.1016/j.biomaterials.2006.12.028.

[28] X. Zhang, Y. Li, Y.E. Chen, J. Chen, P.X. Ma, Cell-free 3D scaffold with two-stage delivery of miRNA-26a to regenerate critical-sized bone defects, Nat. Commun. 7 (1) (2016) 10376, https://doi.org/10.1038/ncomms10376.

[29] M. Dang, A.J. Koh, X. Jin, L.K. McCauley, P.X. Ma, Local pulsatile PTH delivery regenerates bone defects via enhanced bone remodeling in a cell-free scaffold, Biomaterials 114 (2017) 1–9, https://doi.org/10.1016/j.biomaterials.2016.10.049.

[30] M.J. Gupte, W.B. Swanson, J. Hu, X. Jin, H. Ma, Z. Zhang, Z. Liu, K. Feng, G. Feng, G. Xiao, N. Hatch, Y. Mishina, P.X. Ma, Pore size directs bone marrow stromal cell fate and tissue regeneration in nanofibrous macroporous scaffolds by mediating vascularization, Acta Biomater. 82 (2018) 1–11, https://doi.org/10.1016/j.actbio.2018.10.016.

[31] X. Mi, M.J. Gupte, Z. Zhang, W.B. Swanson, L.K. McCauley, P.X. Ma, Three-dimensional electrodeposition of calcium phosphates on porous nanofibrous scaffolds and their controlled release of calcium for bone regeneration, ACS Appl. Mater. Interfaces 12 (29) (2020) 32503–32513, https://doi.org/10.1021/acsami.0c11003.

[32] W. Wang, M. Dang, K. Wang, L. Ni, H. Richie, P.X. Ma, Short-term exposure to TNF-α promotes odontogenesis of stem cells of apical papilla on nanofibrous poly(l-lactic acid) scaffolds, Materialia 32 (2023) 101951, https://doi.org/10.1016/j.mtla.2023.101951.

[33] C.D. Reyes, A.J. García, A2β1 integrin-specific collagen-mimetic surfaces supporting osteoblastic differentiation, J. Biomed. Mater. Res. 69A (4) (2004) 591–600, https://doi.org/10.1002/jbm.a.30034.

[34] A.M. Wojtowicz, A. Shekaran, M.E. Oest, K.M. Dupont, K.L. Templeman, D. W. Hutmacher, R.E. Guldberg, A.J. García, Coating of biomaterial scaffolds with the collagen-mimetic peptide GFOGER for bone defect repair, Biomaterials 31 (9) (2010) 2574–2582, https://doi.org/10.1016/j.biomaterials.2009.12.008.

[35] A. Shekaran, J.R. García, A.Y. Clark, T.E. Kavanaugh, A.S. Lin, R.E. Guldberg, A. J. García, Bone regeneration using an alpha 2 beta 1 integrin-specific hydrogel as a BMP-2 delivery vehicle, Biomaterials 35 (21) (2014) 5453–5461, https://doi.org/10.1016/j.biomaterials.2014.03.055.

[36] C. Ge, Z. Wang, G. Zhao, B. Li, J. Liao, H. Sun, R.T. Franceschi, Discoidin receptor 2 controls bone formation and marrow adipogenesis, J. Bone Miner. Res. 31 (12) (2016) 2193–2203, https://doi.org/10.1002/jbmr.2893.

[37] F. Mohamed, C. Ge, S.A. Hallett, A.C. Bancroft, R.T. Cowling, N. Ono, A.-A. Binrayes, B. Greenberg, B. Levi, V.M. Kaartinen, R.T. Franceschi, Control of craniofacial development by the collagen receptor, discoidin domain receptor 2, Elife 12 (2023), https://doi.org/10.7554/eLife.77257.

[38] F.F. Mohamed, C. Ge, R.T. Cowling, D. Lucas, S.A. Hallett, N. Ono, A.A. Binrayes, B. Greenberg, R.T. Franceschi, The collagen receptor, discoidin domain receptor 2, functions in Gli1-positive skeletal progenitors and chondrocytes to control bone development, Bone Res 10 (1) (2022) 11, https://doi.org/10.1038/s41413-021-00182-w.

[39] A. Binrayes, C. Ge, F.F. Mohamed, R.T. Franceschi, Role of discoidin domain receptor 2 in craniofacial bone regeneration, J. Dent. Res. 100 (12) (2021) 1359–1366, https://doi.org/10.1177/00220345211007447.

[40] S. Bok, A.R. Yallowitz, J. Sun, J. McCormick, M. Cung, L. Hu, S. Lalani, Z. Li, B. R. Sosa, T. Baumgartner, P. Byrne, T. Zhang, K.W. Morse, F.F. Mohamed, C. Ge, R. T. Franceschi, R.T. Cowling, B.H. Greenberg, D.J. Pisapia, T.A. Imahiyerobo, S. Lakhani, M.E. Ross, C.E. Hoffman, S. Debnath, M.B. Greenblatt, A multi-stem cell basis for craniosynostosis and calvarial mineralization, Nature 621 (7980) (2023) 804–812, https://doi.org/10.1038/s41586-023-06526-2.

[41] R. Bargal, V. Cormier-Daire, Z. Ben-Neriah, M. Le Merrer, J. Sosna, J. Melki, D. H. Zangen, S.F. Smithson, Z. Borochowitz, R. Belostotsky, A. Raas-Rothschild, Mutations in DDR2 gene cause SMED with short limbs and abnormal calcifications, Am. J. Hum. Genet. 84 (1) (2009) 80–84, https://doi.org/10.1016/j.ajhg.2008.12.004.

[42] K. Kano, C. Marin de Evsikova, J. Young, C. Wnek, T.P. Maddatu, P.M. Nishina, J. K. Naggert, A novel dwarfism with gonadal dysfunction due to loss-of-function allele of the collagen receptor gene, Ddr2, in the mouse, Mol. Endocrinol. 22 (8) (2008) 1866–1880, https://doi.org/10.1210/me.2007-0310.

[43] H. Xu, D. Bihan, F. Chang, P.H. Huang, R.W. Farndale, B. Leitinger, Discoidin domain receptors promote alpha1beta1- and alpha2beta1-integrin mediated cell adhesion to collagen by enhancing integrin activation, PLoS One 7 (12) (2012) e52209, https://doi.org/10.1371/journal.pone.0052209.

[44] C. Ge, Y. Li, F. Wu, P. Ma, R.T. Franceschi, Synthetic peptides activating discoidin domain receptor 2 and collagen-binding integrins cooperate to stimulate osteoblast differentiation of skeletal progenitor cells, Acta Biomater. 166 (2023) 109–118, https://doi.org/10.1016/j.actbio.2023.05.039.

[45] R. Riva, S. Schmeits, F. Stoffelbach, C. Jérôme, R. Jérôme, P. Lecomte, Combination of ring-opening polymerization and “click” chemistry towards functionalization of aliphatic polyesters, Chem. Commun. (42) (2005) 5334, https://doi.org/10.1039/b510282k.

[46] Z. Zhang, M.J. Gupte, X. Jin, P.X. Ma, Injectable peptide decorated functional nanofibrous hollow microspheres to direct stem cell differentiation and tissue regeneration, Adv. Funct. Mater. 25 (3) (2015) 350–360, https://doi.org/10.1002/adfm.201402618.

[47] K.M. Woo, V.J. Chen, H.-M. Jung, T.-I. Kim, H.-I. Shin, J.-H. Baek, H.-M. Ryoo, P. X. Ma, Comparative evaluation of nanofibrous scaffolding for bone regeneration in critical-size calvarial defects, Tissue Eng. Part A 15 (8) (2009) 2155–2162, https://doi.org/10.1089/ten.tea.2008.0433.

[48] A.B. Lowe, Thiol–ene “click” reactions and recent applications in polymer and materials synthesis: a first update, Polym. Chem. 5 (17) (2014) 4820–4870, https://doi.org/10.1039/c4py00339j.

[49] A.B. Lowe, Thiol-ene “click” reactions and recent applications in polymer and materials synthesis, Polym. Chem. 1 (1) (2010) 17–36.

[50] A.Y. Clark, K.E. Martin, J.R. Garcia, C.T. Johnson, H.S. Theriault, W.M. Han, D. W. Zhou, E.A. Botchwey, A.J. Garcia, Integrin-specific hydrogels modulate transplanted human bone marrow-derived mesenchymal stem cell survival, engraftment, and reparative activities, Nat. Commun. 11 (1) (2020) 114, https://doi.org/10.1038/s41467-019-14000-9.

[51] C.D. Reyes, A.J. Garcia, Alpha2beta1 integrin-specific collagen-mimetic surfaces supporting osteoblastic differentiation, J. Biomed. Mater. Res. 69 (4) (2004) 591–600, https://doi.org/10.1002/jbm.a.30034.

[52] R. Mhanna, E. Ozturk, Q. Vallmajo-Martin, C. Millan, M. Muller, M. Zenobi-Wong, GFOGER-modified MMP-sensitive polyethylene glycol hydrogels induce chondrogenic differentiation of human mesenchymal stem cells, Tissue Eng Part A 20 (7–8) (2014) 1165–1174, https://doi.org/10.1089/ten.TEA.2013.0519.
[53] R. Zhang, P.X. Ma, Synthetic nano-fibrillar extracellular matrices with predesigned macroporous architectures, J. Biomed. Mater. Res. 52 (2) (2000) 430–438, https://doi.org/10.1002/1097-4636(200011)52:2<430::AID-JBM25>3.0.CO;2-L.
[54] G. Wei, P.X. Ma, Structure and properties of nano-hydroxyapatite/polymer composite scaffolds for bone tissue engineering, Biomaterials 25 (19) (2004) 4749–4757, https://doi.org/10.1016/j.biomaterials.2003.12.005.
[55] K.M. Woo, V.J. Chen, P.X. Ma, Nano-fibrous scaffolding architecture selectively enhances protein adsorption contributing to cell attachment, J. Biomed. Mater. Res. 67 (2) (2003) 531–537, https://doi.org/10.1002/jbm.a.10098.
[56] D.W. Hutmacher, Scaffolds in tissue engineering bone and cartilage, Biomaterials 21 (24) (2000) 2529–2543, https://doi.org/10.1016/s0142-9612(00)00121-6.
[57] K.M. Woo, V.J. Chen, H.M. Jung, T.I. Kim, H.I. Shin, J.H. Baek, H.M. Ryoo, P. X. Ma, Comparative evaluation of nanofibrous scaffolding for bone regeneration in critical-size calvarial defects, Tissue Eng Part A 15 (8) (2009) 2155–2162, https://doi.org/10.1089/ten.tea.2008.0433.
[58] X. Zhang, Y. Li, Y.E. Chen, J. Chen, P.X. Ma, Cell-free 3D scaffold with two-stage delivery of miRNA-26a to regenerate critical-sized bone defects, Nat. Commun. 7 (2016) 10376, https://doi.org/10.1038/ncomms10376.
[59] T. Aberg, R. Rice, D. Rice, I. Thesleff, J. Waltimo-Siren, Chondrogenic potential of mouse calvarial mesenchyme, J. Histochem. Cytochem. 53 (5) (2005) 653–663, https://doi.org/10.1369/jhc.4A6518.2005.
[60] L. Yang, K.Y. Tsang, H.C. Tang, D. Chan, K.S. Cheah, Hypertrophic chondrocytes can become osteoblasts and osteocytes in endochondral bone formation, Proc. Natl. Acad. Sci. U.S.A. 111 (33) (2014) 12097–12102, https://doi.org/10.1073/pnas.1302703111.
[61] K.M. Woo, J.-H. Jun, V.J. Chen, J. Seo, J.-H. Baek, H.-M. Ryoo, G.-S. Kim, M. J. Somerman, P.X. Ma, Nano-fibrous scaffolding promotes osteoblast differentiation and biomineralization, Biomaterials 28 (2) (2007) 335–343, https://doi.org/10.1016/j.biomaterials.2006.06.013.
[62] G. Wei, P.X. Ma, Macroporous and nanofibrous polymer scaffolds and polymer/bone-like apatite composite scaffolds generated by sugar spheres, J. Biomed. Mater. Res. 78A (2) (2006) 306–315, https://doi.org/10.1002/jbm.a.30704.
[63] B.S. Kim, A.J. Putnam, T.J. Kulik, D.J. Mooney, Optimizing seeding and culture methods to engineer smooth muscle tissue on biodegradable polymer matrices, Biotechnol. Bioeng. 57 (1) (1998) 46–54, https://doi.org/10.1002/(SICI)1097-0290(19980105)57:1<46::AID-BIT6>3.0.CO;2-V.